International Journal of Non-Linear Mechanics 129 (2021) 103638

Contents lists available at ScienceDirect

International Journal of Non-Linear Mechanics

journal homepage: www.elsevier.com/locate/nlm

A multiphase virtual mass model for debris flow

Parameshwari Kattel [a], Khim B. Khattri [b], Shiva P. Pudasaini [c,d,*]

[a] Department of Mathematics, Tri-Chandra Multiple Campus, Tribhuvan University, Kathmandu, Nepal
[b] Department of Mathematics, School of Science, Kathmandu University, Dhulikhel, Kavrepalanchok, Nepal
[c] Institute of Geosciences, Geophysics Section, University of Bonn, Meckenheimer Allee 176, D-53115, Bonn, Germany
[d] Chair of Landslide Research, Technical University of Munich, Arcisstrasse 21, D-80333 Munich, Germany

ARTICLE INFO

Keywords:
Three-phase mass flow
Multiphase debris flow
Virtual mass forces
Drag
Interphase entrapments

ABSTRACT

In a rapidly moving multiphase mass flow, drag and virtual mass forces are important interfacial forces. However, in many existing literatures, virtual mass force has often been ignored or employed empirically. In this contribution, we construct analytical, full and explicit expressions for the virtual mass coefficients in the true three-phase typical debris flow consisting of coarse-solid, fine-solid and fluid. Similar to virtual mass coefficients, three different linear functions are introduced to connect the volume fractions and velocities of three distinct bulks of phases with other three entrapped fields, namely fine-solid entrapped in coarse-solid, and fluid entrapped in coarse-solid and fine-solid. This results in the emergence of three fundamentally different virtual mass forces expressed as analytical functions of phase-fractions, phase-densities, and the capacity of the solid-type material to hold the fluid-type materials in the mixture. Emergence of the virtual mass force coefficients induced enhanced viscosities, phase fractions, drags, viscous stresses and gravity forces of the coarse-solid and fine-solid indicate the further importance of the newly constructed multiphase mass flow model. For different local distributions of the viscous fluid and the fine particle concentrations, the model can be applied to the different flow regimes of the mixture from dilute to dense so as to cover the whole spectrum of the mixture rheology for each phase limit. In our generic model, entrapment coefficients, viscous rheology and drag coefficients can be used according to the nature of the materials involved and the flow situation. The reductions to existing two-phase mass flow models further indicate that the developed model is more generalized than the existing two-phase models. The reduced virtual mass coefficients for two-phases are still more generalized than the existing two-phase models. The simulation results using the new virtual mass coefficient with two different values of the entrapment coefficients reveal dynamically different flow-obstacle-interactions resulting in more phase-separation for the lower value of the entrapment coefficient.

1. Introduction

Gravitational mass flows, and in particular the debris flows [1–3] can be better and more realistically described by three-phase mass flow models that include viscous fluid, fine-sediments, and coarse-sediments [4] since these three phases possess different rheologies and flow dynamics. A three-phase model with phase transition will also be appropriate to model the mixture flow including rock, ice and viscous fluid [5,6]. Many past researches have treated debris flow as effectively a single mixture flow [1,7] or two-phase flow with solid grains and viscous fluid [8,9]. A significant advancement in two-phase debris flow and simulations is made by Pudasaini [9] by developing a physics-based general mass flow model that includes buoyancy and other three dominant aspects of two-phase mass flow dynamics, namely the non-Newtonian viscous effect due to the gradient of solid volume fraction, generalized drag and the virtual mass. Pudasaini [9], for the first time, included the virtual mass forces to study the two-phase debris flow dynamics.

Drag force describes very important mechanisms of multiphase mass flow as it is also the one that incorporates coupling between the phases through the relative phase velocity [8–10]. Since the drag force becomes dominant as the particle concentration increases up to a certain level, it strongly influences the erosion, lateral levee formation, phase-separation, run out distance, obstacle-interactions, impact pressures on obstacles, and the entire flow dynamics [9–15]. So, more appropriate formulation of drag is needed for better description of the different aspects of multiphase mass flow dynamics [10]. In most of the existing literature, either some empirical values or some simple constitutive equations and models were used to describe the drag force for different types of mass flows [9,16–19]. These previous formulations of drag often lack strong physical basis. Pudasaini [9] proposed a generalized drag that could combine the solid- and fluid-like contributions to drag

* Corresponding author at: Institute of Geosciences, Geophysics Section, University of Bonn, Meckenheimer Allee 176, D-53115, Bonn, Germany.
E-mail address: pudasaini@geo.uni-bonn.de (S.P. Pudasaini).

https://doi.org/10.1016/j.ijnonlinmec.2020.103638
Received 25 June 2020; Received in revised form 7 November 2020; Accepted 8 November 2020
Available online 16 November 2020
0020-7462/

forces. Besides this generalized drag, Kattel et al. [20] and Mergili et al. [21], Mergili et al. [6] also used the ambient drag or air resistance to simulate two-phase flow. In most of the previous models, the drag coefficients increase exponentially along with increasing particle concentrations, arising singularity [8,9,22]. But in reality, a hydrodynamic force cannot be infinitely large. To overcome this case, Pudasaini [10] presented an improved and fully analytical model which is smooth and bounded for the entire domain $[0, 1]$ of solid volume fraction, and also revealed that the maximum value of the drag lies somewhere between the dilute and dense limit of particle concentration. In our work, the drag force that evolves in the model due to the entrapped fluid-type materials in solid-type is generic so that one can use appropriate drag coefficient including that of Pudasaini [10].

Along with the drag, virtual mass force is also a very important component of the interfacial momentum transfer in rapidly accelerating multiphase flows [23]. Virtual mass force is induced in multiphase mass flow due to the non-zero relative acceleration between the phases [17,24–27]. It is the force required to accelerate the apparent mass of the surrounding field (or, phase) due to the relative changes of velocity of the fields, thereby bringing the inertia effect [9,16,23,28]. As for instance, when a solid particle (or a bubble) moves along a quiescent or relatively slowly moving fluid, it also carries some fluid portion along with it so that this portion of fluid mass also attains the particle or bubble velocity, thereby increasing the virtual mass of the particle in the mixture. This also alters the kinetic energy of the fluid motion in the mixture [23,28,29]. Virtual mass term appears in the momentum equations of multiphase mass flow as an important interphase exchange term, not only with its physical significance, but also to more accurately predict the flow variables, including velocity field and pressure [23,28–30], to achieve the mathematical hyperbolicity and numerical stability, and to enhance the computational efficiency of the model by changing the eigenvalues of the system of the partial differential equations comprising the model [24,27,31–33]. However, virtual mass can also be included in mass balance if there is variational formulation of the model available [17]. Model system without virtual mass consideration will be ill-posed with unstable solutions against perturbation, and the model can be made well-posed for certain type and values of the virtual mass coefficient [17,27]. For high speed multiphase flow or a rapid transient problem, virtual mass has crucial role, and therefore cannot be ignored [23,28].

There are significant study of virtual mass, but most of them were in the liquid-gas interfaces mainly in bubbles and liquids [25,34–39]. Most of these works took account of the virtual mass effects as the displacement of liquid when bubbles pass through it [34–36,40]. Cook and Harlow [25], for the first time, modeled the virtual mass as a portion of surrounding fluid entrapped in the bubbles, resulting in the third flow field. Although the model seems to be for multiphase (three-field), but as a true phase wise consideration, it is effectively a two-phase model.

In most of the studies, the virtual mass appears as a coefficient of the difference of velocity gradients (relative acceleration) between the phases. Some literatures treated virtual mass coefficient as a void or shape dependent expression with value < 0.5 [27,41], some used 0.5 for simple motion of a single spherical bubble in an infinite domain with no rotation of particles are considered, or in case of dilute limit of the dispersed particle [17,37,39,41], but sometimes about or higher than 5 for infinite row of bubbles in a tube [37,39,41], and some as a second order tensor (i.e., by a 6×6 matrix with components as inertia coefficients), in case particles have lower degree of symmetry (e.g., ellipsoid) or if particles are allowed to rotate [24,42]. Due to hydrodynamic interactions between the gas bubbles, virtual mass coefficient in bubble-fluid mixture depends on the volumetric gas concentration or void fraction [37]. Some ad-hoc or empirical definitions of virtual mass are found to be used in most of the existing literature [17,37]. Many used the basic model, $C = \frac{1 + 2\alpha_s}{2(1 - \alpha_s)}$, or similar expressions for the virtual mass coefficient (C), where the virtual mass force increases with the increasing solid volume fraction (α_s) in the mixture. This leads to singularity for dense mixture flow, or in particular at those regions where the particle concentration is high enough (i.e., $\alpha_s \to 1$) [9,17,37,39,41]. To remove such singularity, Pudasaini [23] derived a novel analytical expression for the virtual mass force coefficient C as a function of the evolving solid fraction and the density ratio between fluid and solid particles in the mixture. Other features of this new analytical model is that it covers the whole domain (0 to 1) of the dispersed (solid) phase fraction in the mixture; employs dynamical variables, is free of fit parameters; and is sufficiently smooth and physically well bounded. Pudasaini [23] also showed that the maximum value of the virtual mass coefficient lies somewhere in between the dilute and dense limits of the solid fraction distribution.

In general, landslides and debris flows can be treated as a three-phase mixture flow [4] where the fluid phase is a mixture of water and very fine particles (e.g., clay, silt, colloids), and can be described as a viscoplastic material. Similarly, the fine-solid phase may include sand and other particles larger than clay and silt and smaller than gravel that can be treated as Coulomb viscoplastic (or, Herschel-Bulkley, Bingham plastic) material. Coarse materials like boulders, cobbles and gravel can be considered as (coarse-) solid phase and can be treated as Mohr–Coulomb continuum [4,43,44]. As these three phases have different rheology in the mixture, they evolve differently and show different dynamics. Although the addition of one extra phase demands extra equations and several other terms in the model to address mechanical, interfacial and dynamical complexities, the importance lies in the more correct study of multiphase mass flows [4].

Natural reservoirs have two different types of porosity, one as a system of fractures/fissures in rocks and the other as interstitial spaces between the rock matrixes, giving rise to the double porosity [45–47]. In naturally fractured reservoirs, the fractures generally have significantly higher permeability than the matrix. The irregular fractures can be represented by some equivalent homogeneous double porosity systems [45]. Arbogast et al. [46] employed homogenization theory to obtain a general form of the double porosity model for a single phase flow in a naturally fractured reservoir; whereas Bourget et al. [47] presented the model for the microscopic nature of two-phase flow with contrasting hydrodynamic properties (wetting fluid like water, and non-wetting fluid like petroleum hydrocarbons) in the similar environment. Such modelings are found to be successful in the study of petroleum recovery process and prediction of groundwater flow [48]. When the non-wetting fluid first displaces the wetting fluid during the primary drainage process, the wetting phase saturation decreases, but it increases during imbibition process when wetting fluid is added in the medium. Later, in the secondary drainage phase, non-wetting fluid displaces wetting fluid. Such directions of saturation change and saturation history give rise to hysteresis [48,49]. In our work, instead of such pore-level modeling, and the saturation history, we consider the entrapments of fluid in fine-solid, and fluid and fine-solid in solid as some volume fractions of the host phases and all the three phases undergo in motion, primarily due to gravity and pressure. The three phases can have different flow mechanics and rheology, and we give special focus on the evolution of three different virtual mass forces during the flow.

Pudasaini and Mergili [4] developed three-phase mass flow model by extending the general two-phase mass flow model of Pudasaini [9] along with the inclusion of multiphase virtual mass forces and generalized drag. This is the first-ever multi-mechanical, multiphase mass flow model, very flexible to consider and combine more than two phases with different material and flow characteristics arbitrarily. In addition, they performed multiple simulations with eight different mixtures for varied compositions of fluid, fine-solid and solid down a bell-shaped mound and obtained different dynamical behaviors of the phases in the mixture, especially in the deformation, expanding fans, fingering and lobe formation mechanisms and run out distances. They also performed a benchmark test for landslide-reservoir interactions

with a landslide of solid material followed by the other landslide of fine-solid material. However, our approach and the resulting expressions for virtual mass forces here are different. The main purpose of this work is to construct a generic model frame for a multiphase debris flow taking account of the entrapped fluid-type phases in solid-type phase. In the model development process, three linear functions analogous to virtual mass coefficients relate the volume fractions and velocities of the entrapped phases to those of the host phases. The resulting model manifests complex but explicit and generic structures of drag and viscous forces along with legitimate virtual mass forces those emerge in the interfaces between all the pairs of phases. The virtual mas coefficients are further reduced to those for two phases and are compared to the existing coefficients for two-phase mass flows. The newly derived virtual mass coefficient is employed to simulate two-phase debris flow, where two different entrapment coefficients produce different flow dynamics and obstacle-interactions.

2. A three-phase six-field debris flow model

2.1. The six field quantities

The notations, variables and parameters have been defined in the Section 'List of Symbols'. In our three-phase mass flow model, we denote the coarse-solid, fine-solid and fluid phases by the subscripts s, fs and f, respectively. Each phase is considered to be incompressible. The superscript e_s has been used for the entrapped fluid or fine-solid in coarse-solid, and e_{fs} for the fluid entrapped in fine-solid. Let α_i denote the volume fraction of the phase i ($i = s$, fs or f) in the debris mixture. Then, due to the volume conservation, we have the following hold-up relation:

$$\alpha_s + \alpha_{fs} + \alpha_f = 1. \tag{1}$$

In the mixture, a certain portion of the fine-sediments can be entrapped in solid (coarse-solid). So, the sum of the portion of the fine-solid material contained in its own bulk ($\bar{\alpha}_{fs}$) and the other portion of fine-solid entrapped in solid ($\alpha_{fs}^{e_s}$) will sum to the portion of the total (actual) fine-solid in the mixture:

$$\bar{\alpha}_{fs} + \alpha_{fs}^{e_s} = \alpha_{fs}. \tag{2}$$

In the same way, as the fluid can be entrapped in both solid and the fine-solid phases, the fluid portion in its own bulk ($\bar{\alpha}_f$), the fluid entrapped in solid ($\alpha_f^{e_s}$), and the fluid entrapped in fine-solid ($\alpha_f^{e_{fs}}$) will sum to the total fluid in the mixture:

$$\bar{\alpha}_f + \alpha_f^{e_s} + \alpha_f^{e_{fs}} = \alpha_f. \tag{3}$$

Using (2) and (3) in (1), we have the following equivalent hold-up relation in terms of bulk and entrapped materials:

$$\alpha_s + (\bar{\alpha}_{fs} + \alpha_{fs}^{e_s}) + (\bar{\alpha}_f + \alpha_f^{e_s} + \alpha_f^{e_{fs}}) = 1 \cdot \tag{4}$$

For the solid phase, its volume fraction and the bulk are the same (i.e., $\bar{\alpha}_s = \alpha_s$). Now, we have the six fields, namely coarse-solid, bulk fine-solid, bulk fluid, fine-solid entrapped in coarse-solid, fluid entrapped in coarse-solid and fluid entrapped in fine-solid (see, Fig. 1) in the mixture. Henceforth, by solid, we mean the coarse-solid.

Let $\bar{\mathbf{u}}_s, \bar{\mathbf{u}}_{fs}$ and $\bar{\mathbf{u}}_f$ denote the respective velocities of the bulk solid, bulk fine-solid and bulk fluid; $\mathbf{u}_{fs}^{e_s}, \mathbf{u}_f^{e_s}$ denote the velocities of the entrapped fine-solid and fluid in solid, and $\mathbf{u}_f^{e_{fs}}$ denote the velocity of fluid entrapped in fine-solid. Since the total momentum of fine-solid and fluid phases are the sum of the separate momenta contained in the respective bulk phases and the entrapped fields, we have the following two relations for fine-solid and fluid momentum, respectively.

$$\alpha_{fs}\mathbf{u}_{fs} = \bar{\alpha}_{fs}\bar{\mathbf{u}}_{fs} + \alpha_{fs}^{e_s}\mathbf{u}_{fs}^{e_s}, \tag{5}$$

$$\alpha_f\mathbf{u}_f = \bar{\alpha}_f\bar{\mathbf{u}}_f + \alpha_f^{e_s}\mathbf{u}_f^{e_s} + \alpha_f^{e_{fs}}\mathbf{u}_f^{e_{fs}}. \tag{6}$$

But, the bulk momentum of solid remains unchanged:

$$\alpha_s\mathbf{u}_s = \bar{\alpha}_s\bar{\mathbf{u}}_s. \tag{7}$$

Now, the relations (5)–(7) are employed to generate six equations for mass and the other six equations for momentum balances for the newly defined field variables on the right hand sides of (5)–(7).

2.2. Mass balance equations

We begin with the following six mass balance equations for the six fields: solid, fine-solid entrapped in solid, fluid entrapped in solid, bulk fine-solid, fluid entrapped in fine-solid, and bulk fluid respectively.

$$\frac{\partial}{\partial t}(\rho_s\alpha_s) + \nabla\cdot(\rho_s\alpha_s\mathbf{u}_s) = 0, \tag{8}$$

$$\frac{\partial}{\partial t}(\rho_{fs}\alpha_{fs}^{e_s}) + \nabla\cdot(\rho_{fs}\alpha_{fs}^{e_s}\mathbf{u}_{fs}^{e_s}) = 0, \tag{9}$$

$$\frac{\partial}{\partial t}(\rho_f\alpha_f^{e_s}) + \nabla\cdot(\rho_f\alpha_f^{e_s}\mathbf{u}_f^{e_s}) = 0, \tag{10}$$

$$\frac{\partial}{\partial t}(\rho_{fs}\bar{\alpha}_{fs}) + \nabla\cdot(\rho_{fs}\bar{\alpha}_{fs}\bar{\mathbf{u}}_{fs}) = 0, \tag{11}$$

$$\frac{\partial}{\partial t}(\rho_f\alpha_f^{e_{fs}}) + \nabla\cdot(\rho_f\alpha_f^{e_{fs}}\mathbf{u}_f^{e_{fs}}) = 0, \tag{12}$$

$$\frac{\partial}{\partial t}(\rho_f\bar{\alpha}_f) + \nabla\cdot(\rho_f\bar{\alpha}_f\bar{\mathbf{u}}_f) = 0. \tag{13}$$

We note that the Eqs. (8), (11) and (13) are somehow related to the original mass balance equations for solid, fine-solid and fluid, which would regenerate into the original mass balance equations if there were no entrapped materials. Eqs. (9), (10) and (12) are completely new mass balance equations induced by the entrapped materials that would have ceased to exist, had there been no entrapped materials.

A. Mass Balance for Solid:

Since the solid is not entrapped in other phases, the solid mass balance equation is simply Eq. (8), which is

$$\frac{\partial}{\partial t}(\rho_s\alpha_s) + \nabla\cdot(\rho_s\alpha_s\mathbf{u}_s) = 0. \tag{14}$$

B. Mass Balance for Fine-solid:

We add (9) and (11), and use (2) and (5) to get the following mass balance equation for the total fine-solid phase.

$$\frac{\partial}{\partial t}(\rho_{fs}\alpha_{fs}) + \nabla\cdot(\rho_{fs}\alpha_{fs}\mathbf{u}_{fs}) = 0. \tag{15}$$

C. Mass Balance for Fluid:

Next, we add (10), (12) and (13), and use (3) and (6) to get the following analogous mass balance equation for the total fluid phase.

$$\frac{\partial}{\partial t}(\rho_f\alpha_f) + \nabla\cdot(\rho_f\alpha_f\mathbf{u}_f) = 0. \tag{16}$$

In this way, (14)–(16) appear as the usual three-phase mass balance equations for the solid, fine-solid and the fluid phases, respectively. These three equations along with the three momentum balance equations that we construct in the next section will form a complete model system for a true three-phase mass flow.

2.3. Momentum balance equations

A. Velocity Estimation of Entrapped Materials:

It is legitimate to consider that each entrapped fluid-type material moves along with the solid-type material that entraps it. So, in (9)–(12), we can approximate the velocities as:

$$\mathbf{u}_f^{e_s} \approx \mathbf{u}_{fs}^{e_s} \approx \mathbf{u}_s, \tag{17}$$

and

$$\mathbf{u}_f^{e_{fs}} \approx \bar{\mathbf{u}}_{fs}. \tag{18}$$

B. Emergence of the Virtual Mass Coefficients due to Entrapped Fields:

Since solid can entrap a certain portion of fine-solid and fluid, and fine-solid can entrap a certain portion of fluid, we can express the

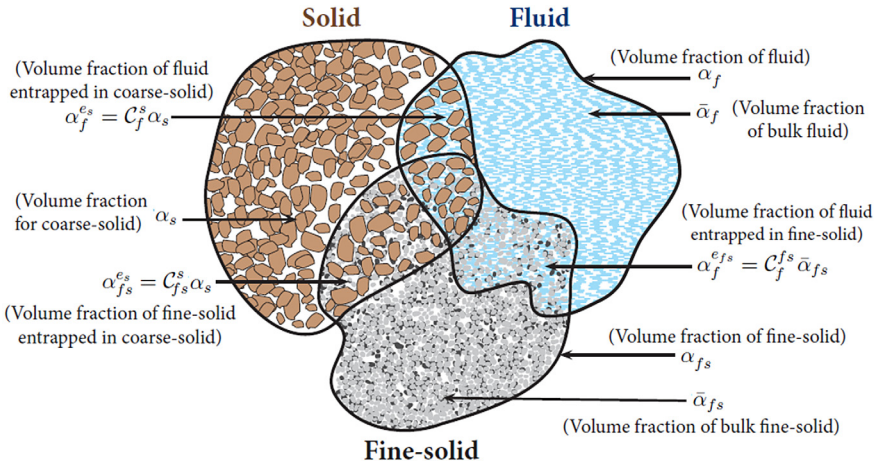

Fig. 1. A sketch showing the three phases and six fields in a three-phase debris mixture. α_s, α_{fs} and α_f are the volume fractions of solid, fine-solid and fluid in the mixture. The fine-solid phase is divided into the two fields, namely the fine-solid entrapped in solid and bulk fine-solid. Similarly, the fluid phase is divided into the three fields, namely the fluid entrapped in solid, fluid entrapped in fine-solid and bulk fluid. The fractions of fine-solid entrapped in solid, fluid entrapped in solid and fluid entrapped in bulk fine-solid are denoted by C_{fs}^s, C_f^s and C_f^{fs}, respectively.

volume fraction of the entrapped material as a certain fraction of the actual volume fraction of the host phase, and so as a certain fraction of the respective bulk materials [25]. In particular, as $\alpha_{fs} = \alpha_{fs}^{e_s} + \bar{\alpha}_{fs}$, $\bar{\alpha}_{fs}$ is a certain fraction of α_{fs}. Again since $\alpha_f^{e_{fs}}$ is a certain fraction of α_{fs}, $\alpha_f^{e_{fs}}$ is also a certain fraction of $\bar{\alpha}_{fs}$. So, we have:

$$\alpha_{fs}^{e_s} = C_{fs}^s \alpha_s; \quad \alpha_f^{e_s} = C_f^s \alpha_s; \quad \alpha_f^{e_{fs}} = C_f^{fs} \bar{\alpha}_{fs}. \tag{19}$$

The functions C those appear in (19) depend on the relative velocity between the phases, and geometry and number of the dispersed particles in the flow [23,25,39,41]. Analogous to virtual mass coefficient C_{VM} in [9], all C functions in (19) are expressed in relation to the solid (-type) material entrapping the surrounding fluid (-type) materials. We note that the definitions of virtual mass force coefficients in (19) are legitimate. Because, for example, as solid entraps fine-solid, the solid-phase must now accelerate the additional entrapped fine-solid. This changes the inertia of the solid phase and thus induces the virtual mass. The same is true for other entrapments. Introduction of the virtual mass coefficients is also important, because, with this, now we can relate bulk fluid and bulk fine-solid momenta with the solid, total fine-solid and total fluid momenta, which we will use to construct the momentum equations of the three phases.

From (5), (17) and (19), we have

$$\bar{\alpha}_{fs}\, \bar{\mathbf{u}}_{fs} = \alpha_{fs}\, \mathbf{u}_{fs} - C_{fs}^s\, \alpha_s\, \mathbf{u}_s. \tag{20}$$

Similarly, from (6), and (17)–(20) (Full derivation is shown in Supplementary Materials.), we have

$$\bar{\alpha}_f\, \bar{\mathbf{u}}_f = \alpha_f\, \mathbf{u}_f - \left(C_f^s - C_f^{fs} C_{fs}^s\right) \alpha_s\, \mathbf{u}_s - C_f^{fs} \alpha_{fs}\, \mathbf{u}_{fs}. \tag{21}$$

Thus, the bulk fine-solid and bulk fluid fluxes are now expressed in terms of the solid, total fine-solid and total fluid fluxes together with the linear (C_{fs}^s, C_f^s, C_f^{fs}), and non-linear ($C_f^s C_{fs}^s$) combinations of virtual mass coefficients. We need the relations (20) and (21) later to construct the momentum equations for fine-solid (37) and for fluid (40) with enhanced densities.

C. Relative Bulk Velocities in terms of Relative Phase Velocities

Below, we express the differences of the bulk velocities in terms of the differences of phase velocities, which we need for the drag terms in the upcoming momentum equations. For this, we use the expressions for the bulk velocities in terms of the phase velocities obtained in (20) and (21):

$$\bar{\mathbf{u}}_{fs} - \mathbf{u}_s = \frac{\alpha_{fs}(\mathbf{u}_{fs} - \mathbf{u}_s)}{\alpha_{fs} - C_{fs}^s \alpha_s}, \tag{22}$$

$$\bar{\mathbf{u}}_f - \mathbf{u}_s = \frac{\alpha_f(\mathbf{u}_f - \mathbf{u}_s) + C_f^{fs} \alpha_{fs} \left(\mathbf{u}_s - \mathbf{u}_{fs}\right)}{\alpha_f - C_f^{fs} \alpha_{fs} - (C_f^s - C_f^{fs} C_{fs}^s)\alpha_s}, \tag{23}$$

$$\bar{\mathbf{u}}_f - \bar{\mathbf{u}}_{fs} = \frac{\alpha_f\, \alpha_{fs}(\mathbf{u}_f - \mathbf{u}_{fs}) - C_f^s \alpha_s\, \alpha_{fs}\, (\mathbf{u}_s - \mathbf{u}_{fs}) - C_{fs}^s \alpha_f \alpha_s (\mathbf{u}_f - \mathbf{u}_s)}{(\alpha_f - C_f^{fs} \alpha_{fs} - (C_f^s - C_f^{fs} C_{fs}^s)\, \alpha_s)(\alpha_{fs} - C_{fs}^s \alpha_s)}. \tag{24}$$

Thus, with the help of the expressions for the fluxes of the bulk phases, we have expressed the relative bulk velocities in terms of the relative actual phase velocities. In fact, these relative velocities differ from the usual relative velocities due to the changes in inertia emerging from the entrapments.

Next, we construct the momentum balances for all the three phases from the balances of the bulks and the entrapped fluid-type materials.

2.3.1. Momentum balance equations for solid and entrapped fluid-type materials

Now, we write the momentum equations for solid, and the fluid type materials entrapped in solid, i.e., entrapped fine-solid and fluid in solid. Later in this Section, we combine them into a single momentum equation for solid with entrapments.

$$\begin{aligned}
&\frac{\partial}{\partial t}(\rho_s \alpha_s \mathbf{u}_s) + \nabla \cdot (\rho_s \alpha_s \mathbf{u}_s\, \mathbf{u}_s) = -\alpha_s \nabla p + \rho_s \alpha_s \mathbf{g} \\
&+ K_{\mathrm{s}}^{\mathrm{fs}}(\bar{\mathbf{u}}_{fs} - \mathbf{u}_s) + K_{\mathrm{s}}^{\mathrm{f}}(\bar{\mathbf{u}}_f - \mathbf{u}_s) + K_{\mathrm{s}}^{\text{f-efs}}(\mathbf{u}_f^{e_{fs}} - \mathbf{u}_s) + V_s,
\end{aligned} \tag{25}$$

$$\begin{aligned}
&\frac{\partial}{\partial t}(\rho_{fs} \alpha_{fs}^{e_s} \mathbf{u}_{fs}^{e_s}) + \nabla \cdot (\rho_{fs} \alpha_{fs}^{e_s} \mathbf{u}_{fs}^{e_s}\, \mathbf{u}_{fs}^{e_s}) = -\alpha_{fs}^{e_s} \nabla p + \rho_{fs} \alpha_{fs}^{e_s} \mathbf{g} \\
&+ K_{\text{fs-es}}^{\mathrm{fs}}(\bar{\mathbf{u}}_{fs} - \mathbf{u}_{fs}^{e_s}) + K_{\text{fs-es}}^{\mathrm{f}}(\bar{\mathbf{u}}_f - \mathbf{u}_{fs}^{e_s}) + K_{\text{fs-es}}^{\text{f-efs}}(\mathbf{u}_f^{e_{fs}} - \mathbf{u}_{fs}^{e_s}) + V_{fs}^{e_s},
\end{aligned} \tag{26}$$

$$\begin{aligned}
&\frac{\partial}{\partial t}(\rho_f \alpha_f^{e_s} \mathbf{u}_f^{e_s}) + \nabla \cdot (\rho_f \alpha_f^{e_s} \mathbf{u}_f^{e_s}\, \mathbf{u}_f^{e_s}) = -\alpha_f^{e_s} \nabla p + \rho_f \alpha_f^{e_s} \mathbf{g} + K_{\text{f-es}}^{\mathrm{f}}(\bar{\mathbf{u}}_{\mathrm{f}} - \mathbf{u}_f^{e_s}) \\
&+ K_{\text{f-es}}^{\mathrm{fs}}(\bar{\mathbf{u}}_{fs} - \mathbf{u}_f^{e_s}) + K_{\text{f-es}}^{\text{f-efs}}(\mathbf{u}_f^{e_{fs}} - \mathbf{u}_f^{e_s}) + V_f^{e_s},
\end{aligned} \tag{27}$$

where V_{s}, $V_{fs}^{e_s}$ and $V_f^{e_s}$ account for the momentum transfer due to the viscosities of the respective fields; the second terms in the right hand sides associated to $\mathbf{g}$ are the gravity terms; and the first terms associated to ∇p are the pressure gradient terms. Moreover, the pressure p is supposed to be locally the same for all the six fields [9,17,25]. The terms associated to K are mainly the drag forces that evolve due to the difference of the velocities of the fields. For example, $K_{\mathrm{s}}^{\mathrm{f}}$ denotes the function for the solid and the bulk fluid, and $K_{\text{f-es}}^{\text{f-efs}}$ denotes that for fluid entrapped in solid and fluid entrapped in fine-solid. These functions

mainly rely on the relative velocities and volume fractions. A simple drag function can be defined as:

$$K_{\rm s}^{\rm f} = \frac{\alpha_s \bar{\alpha}_f (\rho_s - \rho_f) g}{|\bar{\mathbf{u}}_f - \mathbf{u}_s|}.$$

Or, it can be a more generalized one as described in [9]:

$$K_{\rm s}^{\rm f} = \frac{\alpha_s \bar{\alpha}_f (\rho_s - \rho_f) g}{\left[\mathcal{U}_\tau^{s,f}\{\mathcal{P}_s^f \mathcal{F}_s^f(Re_p^{s,f}) + (1-\mathcal{P}_s^f)\mathcal{G}_s^f(Re_p^{s,f})\}\right]^J} |\bar{\mathbf{u}}_f - \mathbf{u}_s|^{J-1}, \tag{28}$$

where the particle Reynolds number $Re_p^{s,f} = \frac{\rho_f d_s \mathcal{U}_\tau^{s,f}}{\eta_f}$, η_f is the fluid viscosity; the terminal velocity of a freely falling coarse-solid particle in a fluid, $\mathcal{U}_\tau^{s,f} = \sqrt{\frac{g d_s \rho_s}{\rho_f}}$, d_s is the particle diameter of a coarse-solid, and $\mathcal{F}_s^f = \left(\frac{\rho_f}{\rho_s}\right)\left(\frac{\bar{\alpha}_f}{\alpha_s}\right)^3 \frac{Re_p^{s,f}}{180}$ and $\mathcal{G}_s^f = \alpha_f^{M(Re_p^{s,f})-1}$ are the solid and fluid like contributions to drag by the interpolation parameter $\mathcal{P}_s^f \in [0,1]$. In the drag formulations of the existing models [8,9,22], the drag coefficient shows the singularity as $\alpha_s \to 1$. Pudasaini [10] formulated the drag force in such a way that a smoothing or a damping function emerges, which removes the singularity. Previously, in [9], $\mathcal{P}_s^f$ was just some numerical value within 0 and 1, whereas in [10] it is a dynamical variable $\mathcal{P}_s^f = \alpha_s^n$, where n is a positive real number so that $\mathcal{P}_s^f$ still lies in $[0,1]$. With these improvements, Pudasaini [10] called this new drag coefficient (28) as the enhanced generalized drag coefficient. For different values of the index n, Pudasaini [10] found that the drag coefficients increase for up to a certain value of α_s, and then decrease again; in the limits $\alpha_s \to 0$ and 1, the drag coefficients vanish naturally. So, the drag force is well bounded. Pudasaini [10] also analyzed different parameters involved in the drag coefficients. Lower values of the terminal velocity produced higher drags, and higher the density ratios of fluid to solid, lower were the drag values.

Other drag terms in (25)–(27) can similarly be defined. However, in the drag term $K_{\text{f-es}}^{\text{f-efs}}$, the difference of the same density of fluid makes it zero. Similarly, other drag terms that include the same fluid-type materials will also be zero. So, the above set of Eqs. (25)–(27) can be rewritten with fewer drag terms:

$$\frac{\partial}{\partial t}(\rho_s \alpha_s \mathbf{u}_s) + \nabla\cdot(\rho_s \alpha_s \mathbf{u}_s \mathbf{u}_s) = -\alpha_s \nabla p + \rho_s \alpha_s \mathbf{g} + K_{\rm s}^{\rm fs}(\bar{\mathbf{u}}_{fs} - \mathbf{u}_s) + K_{\rm s}^{\rm f}(\bar{\mathbf{u}}_f - \mathbf{u}_s) + K_{\rm s}^{\text{f-efs}}(\mathbf{u}_f^{e_{fs}} - \mathbf{u}_s) + V_s, \tag{29}$$

$$\frac{\partial}{\partial t}(\rho_{fs} \alpha_{fs}^{e_s} \mathbf{u}_{fs}^{e_s}) + \nabla\cdot(\rho_{fs} \alpha_{fs}^{e_s} \mathbf{u}_{fs}^{e_s} \mathbf{u}_{fs}^{e_s}) = -\alpha_{fs}^{e_s} \nabla p + \rho_{fs} \alpha_{fs}^{e_s} \mathbf{g} + K_{\text{fs-es}}^{\rm f}(\bar{\mathbf{u}}_f - \mathbf{u}_{fs}^{e_s}) + K_{\text{fs-es}}^{\text{f-efs}}(\mathbf{u}_f^{e_{fs}} - \mathbf{u}_{fs}^{e_s}) + V_{fs}^{e_s}, \tag{30}$$

$$\frac{\partial}{\partial t}(\rho_f \alpha_f^{e_s} \mathbf{u}_f^{e_s}) + \nabla\cdot(\rho_f \alpha_f^{e_s} \mathbf{u}_f^{e_s} \mathbf{u}_f^{e_s}) = -\alpha_f^{e_s} \nabla p + \rho_f \alpha_f^{e_s} \mathbf{g} + K_{\text{f-es}}^{\rm fs}(\bar{\mathbf{u}}_{fs} - \mathbf{u}_f^{e_s}) + V_f^{e_s}, \tag{31}$$

It is interesting to note that there are no virtual mass forces in (29)–(31). Later, we will see how the entrapped materials induce virtual mass forces.

Summing up the first terms on the left hand sides of (29)–(31), and using (17) and (19), we get

$$\frac{\partial}{\partial t}\left(\rho_s \alpha_s \mathbf{u}_s + \rho_{fs} \alpha_{fs}^{e_s} \mathbf{u}_{fs}^{e_s} + \rho_f \alpha_f^{e_s} \mathbf{u}_f^{e_s}\right) = \frac{\partial}{\partial t}(\rho_s^e \alpha_s \mathbf{u}_s), \tag{32a}$$

where $\rho_s^e = \rho_s + \rho_{fs} C_{fs}^s + \rho_f C_f^s$ is now the effective solid density. So, (32a) shows that the solid inertia is increased due to the entrapped fine-solid and fluid in solid.

Similarly, the second terms of the left hand sides of (29)–(31) can be summed up to give

$$\nabla\cdot(\rho_s \alpha_s \mathbf{u}_s \mathbf{u}_s + \rho_{fs} \alpha_{fs}^{e_s} \mathbf{u}_{fs}^{e_s} \mathbf{u}_{fs}^{e_s} + \rho_f \alpha_f^{e_s} \mathbf{u}_f^{e_s} \mathbf{u}_f^{e_s}) \approx \nabla\cdot(\rho_s^e \alpha_s \mathbf{u}_s \mathbf{u}_s). \tag{32b}$$

Moreover, the first terms on the right hand sides of (29)–(31) related to pressure gradients are added to obtain

$$-(\alpha_s + \alpha_{fs}^{e_s} + \alpha_f^{e_s})\nabla p = -(\alpha_s + C_{fs}^s \alpha_s + C_f^s \alpha_s)\nabla p = -\alpha_s^e \nabla p, \tag{32c}$$

where $\alpha_s^e = (1 + C_{fs}^s + C_f^s)\,\alpha_s$ is the effective solid volume fraction in the mixture which is enhanced due to the entrapped fields as indicated by C_{fs}^s and C_f^s.

The gravity terms when combined yield:

$$(\rho_s \alpha_s + \rho_{fs} \alpha_{fs}^{e_s} + \rho_f \alpha_f^{e_s})\,\mathbf{g} = (\rho_s + \rho_{fs} C_{fs}^s + \rho_f C_f^s)\,\alpha_s \mathbf{g} = \rho_s^e \alpha_s \mathbf{g}. \tag{32d}$$

Summing up the drag terms of the right hand sides of (29)–(31), and using the results obtained in (22)–(24), the total drag force will be

$$(K_{\rm s}^{\rm fs} + K_{\rm s}^{\text{f-efs}} + K_{\text{fs-es}}^{\text{f-efs}} + K_{\text{f-es}}^{\rm fs})(\bar{\mathbf{u}}_{fs} - \mathbf{u}_s) + (K_{\rm s}^{\rm f} + K_{\text{fs-es}}^{\rm f})(\bar{\mathbf{u}}_f - \mathbf{u}_s) = \mathcal{K}_d^1 \frac{\alpha_{fs}(\mathbf{u}_{fs} - \mathbf{u}_s)}{\alpha_{fs} - C_{fs}^s \alpha_s} + \mathcal{K}_d^2 \left[\frac{\alpha_f(\mathbf{u}_f - \mathbf{u}_s) + C_f^{fs}\alpha_{fs}(\mathbf{u}_s - \mathbf{u}_{fs})}{(\alpha_f - C_f^{fs}\alpha_{fs} - (C_f^s - C_f^{fs}C_{fs}^s)\alpha_s)}\right], \tag{32e}$$

where $\mathcal{K}_d^1 = K_{\rm s}^{\rm fs} + K_{\rm s}^{\text{f-efs}} + K_{\text{fs-es}}^{\text{f-efs}} + K_{\text{f-es}}^{\rm fs}$, and $\mathcal{K}_d^2 = K_{\rm s}^{\rm f} + K_{\text{fs-es}}^{\rm f}$ are the resultant binary drag coefficients for solid and the fields entrapped in solid with relative to the fine-solid and fluid entrapped in fine-solid and, the fluid respectively. The viscous terms will sum to $V_s + V_{fs}^{e_s} + V_f^{e_s} = V_s^e$, the effective viscous force for solid. Different solid-like and fluid-like or mixed-type viscous forces can be applied for solid, fine-solid and fluid phases, and entrapped materials [9,43,44,50–52]. However, here, we do not explicitly deal with the type of viscous forces, but only deal them intrinsically. Our main focus is to construct in the general and explicit structures of the drag and the virtual mass forces that are induced by the entrapped materials.

Solid Momentum Equation with Enhanced Density: Collecting all the terms from (32a)–(32e) and the viscous forces, we have the solid momentum equation:

$$\frac{\partial}{\partial t}(\rho_s^e \alpha_s \mathbf{u}_s) + \nabla\cdot(\rho_s^e \alpha_s \mathbf{u}_s \mathbf{u}_s) = -\alpha_s^e \nabla p + \rho_s^e \alpha_s \mathbf{g} + \mathcal{K}_d^1 \frac{\alpha_{fs}(\mathbf{u}_{fs} - \mathbf{u}_s)}{\alpha_{fs} - C_{fs}^s \alpha_s} + \mathcal{K}_d^2 \frac{\alpha_f(\mathbf{u}_f - \mathbf{u}_s) + C_f^{fs}\alpha_{fs}(\mathbf{u}_s - \mathbf{u}_{fs})}{(\alpha_f - C_f^{fs}\alpha_{fs} - (C_f^s - C_f^{fs}C_{fs}^s)\alpha_s)} + V_s^e. \tag{33}$$

In (33), due to the entrapped fluid-type materials, there is enhanced density in the inertial and gravity terms, enhanced solid volume fraction in the pressure gradient term, and viscous force has also been enhanced. Clearly, if all the entrapments are ignored, the inertial, pressure, gravity, drag and viscous forces all become the respective usual forces.

2.3.2. Momentum equations for bulk fine-solid and fluid entrapped in fine-solid

Next, we construct similar momentum equation for fine-solid. For this, we write the respective momentum equations for bulk fine-solid and the fluid entrapped in bulk fine-solid:

$$\frac{\partial}{\partial t}(\rho_{fs} \bar{\alpha}_{fs} \bar{\mathbf{u}}_{fs}) + \nabla\cdot(\rho_{fs} \bar{\alpha}_{fs} \bar{\mathbf{u}}_{fs} \bar{\mathbf{u}}_{fs}) = -\bar{\alpha}_{fs} \nabla p + \rho_{fs} \bar{\alpha}_{fs} \mathbf{g} + K_{\rm s}^{\rm fs}(\mathbf{u}_s - \bar{\mathbf{u}}_{fs}) + K_{\text{f-es}}^{\rm fs}(\mathbf{u}_f^{e_s} - \bar{\mathbf{u}}_{fs}) + K_{\rm f}^{\rm fs}(\bar{\mathbf{u}}_f - \bar{\mathbf{u}}_{fs}) + V_{fs}, \tag{34}$$

$$\frac{\partial}{\partial t}(\rho_f \alpha_f^{e_{fs}} \bar{\mathbf{u}}_{fs}) + \nabla\cdot(\rho_f \alpha_f^{e_{fs}} \bar{\mathbf{u}}_{fs} \bar{\mathbf{u}}_{fs}) = -\alpha_f^{e_{fs}} \nabla p + \rho_f \alpha_f^{e_{fs}} \mathbf{g} + K_{\rm s}^{\text{f-efs}}(\mathbf{u}_s - \mathbf{u}_f^{e_{fs}}) + K_{\text{fs-es}}^{\text{f-efs}}(\mathbf{u}_{fs}^{e_s} - \mathbf{u}_f^{e_{fs}}) + V_f^{e_{fs}}. \tag{35}$$

When we add (34) and (35) term by term and use (20), the left hand side becomes

$$\frac{\partial}{\partial t}\left(\rho_{fs} \bar{\alpha}_{fs} \bar{\mathbf{u}}_{fs} + \rho_f \alpha_f^{e_{fs}} \bar{\mathbf{u}}_{fs}\right) + \nabla\cdot\left(\rho_{fs} \bar{\alpha}_{fs} \bar{\mathbf{u}}_{fs}^2 + \rho_f \alpha_f^{e_{fs}} \bar{\mathbf{u}}_{fs}^2\right) = \frac{\partial}{\partial t}\left[\rho_{fs}^e(\alpha_{fs}\mathbf{u}_{fs} - C_{fs}^s \alpha_s \mathbf{u}_s)\right] + \nabla\cdot(\rho_{fs}^e \bar{\alpha}_{fs} \bar{\mathbf{u}}_{fs}^2) = \frac{\partial}{\partial t}\left[\rho_{fs}^e(\alpha_{fs}\mathbf{u}_{fs} - C_{fs}^s \alpha_s \mathbf{u}_s)\right] + \nabla\cdot\frac{\rho_{fs}^e(\alpha_{fs}\mathbf{u}_{fs} - C_{fs}^s \alpha_s \mathbf{u}_s)^2}{(\alpha_{fs} - C_{fs}^s \alpha_s)}, \tag{36a}$$

where $\rho_{fs}^e = (\rho_{fs} + \rho_f C_f^{fs})$ is the effective density for fine-solid which accounts for the fine-solid density enhanced by the density of the fluid entrapped in the fine-solid.

The first and second terms of the right hand sides of (34) and (35) will sum to

$$-(\bar{\alpha}_{fs}+\alpha_f^{e_{fs}})\nabla p+(\rho_{fs}\bar{\alpha}_{fs}+\rho_f\alpha_f^{e_{fs}})\,\mathbf{g}=-(1+C_f^{fs})\,(\alpha_{fs}-C_{fs}^{s}\alpha_s)\nabla p + \rho_{fs}^{e}(\alpha_{fs}-C_{fs}^{s}\alpha_s)\,\mathbf{g}. \tag{36b}$$

Similarly, the last terms of the right hand sides of (34) and (35) after using (22)–(24) will sum to

$$(K_{\mathrm{s}}^{\mathrm{fs}}+K_{\text{f-es}}^{\mathrm{fs}}+K_{\mathrm{s}}^{\text{f-efs}}+K_{\text{fs-es}}^{\text{f-efs}})(\mathbf{u}_s-\bar{\mathbf{u}}_{fs})+K_{\mathrm{f}}^{\mathrm{fs}}(\bar{\mathbf{u}}_f-\bar{\mathbf{u}}_{fs})=\mathcal{K}_d^1\frac{\alpha_{fs}(\mathbf{u}_s-\mathbf{u}_{fs})}{\alpha_{fs}-C_{fs}^{s}\alpha_s} +\mathcal{K}_d^3\frac{\alpha_f\,\alpha_{fs}(\mathbf{u}_f-\mathbf{u}_{fs})-C_f^s\alpha_s\,\alpha_{fs}\,(\mathbf{u}_s-\mathbf{u}_{fs})-C_{fs}^{s}\alpha_f\alpha_s(\mathbf{u}_f-\mathbf{u}_s)}{(\alpha_f-C_f^{fs}\alpha_{fs}-(C_f^s-C_f^{fs}C_{fs}^{s})\alpha_s)(\alpha_{fs}-C_{fs}^{s}\alpha_s)}, \tag{36c}$$

where $\mathcal{K}_d^3=K_{\mathrm{f}}^{\mathrm{fs}}$. Furthermore, the viscous term will be $V_{fs}+V_f^{e_{fs}}=V_{fs}^{e}$, which is the effective viscous force for the fine-solid.

Fine-solid Momentum Equation with Enhanced Density: Collecting all the terms from (36a)–(36c), we have the fine-solid momentum equation:

$$\frac{\partial}{\partial t}\left(\rho_{fs}^{e}(\alpha_{fs}\mathbf{u}_{fs}-C_{fs}^{s}\alpha_s\mathbf{u}_s)\right)+\nabla\cdot\frac{\rho_{fs}^{e}(\alpha_{fs}\mathbf{u}_{fs}-C_{fs}^{s}\alpha_s\mathbf{u}_s)^2}{\alpha_{fs}-C_{fs}^{s}\alpha_s} =-\left(1+C_f^{fs}\right)\left(\alpha_{fs}-C_{fs}^{s}\alpha_s\right)\nabla p+\rho_{fs}^{e}\left(\alpha_{fs}-C_{fs}^{s}\alpha_s\right)\mathbf{g}+\mathcal{K}_d^1\left[\frac{\alpha_{fs}(\mathbf{u}_s-\mathbf{u}_{fs})}{\alpha_{fs}-C_{fs}^{s}\alpha_s}\right] +\mathcal{K}_d^3\left[\frac{\alpha_f\,\alpha_{fs}(\mathbf{u}_f-\mathbf{u}_{fs})-C_f^s\alpha_s\,\alpha_{fs}\,(\mathbf{u}_s-\mathbf{u}_{fs})-C_{fs}^{s}\alpha_f\alpha_s(\mathbf{u}_f-\mathbf{u}_s)}{(\alpha_f-C_f^{fs}\alpha_{fs}-(C_f^s-C_f^{fs}C_{fs}^{s})\alpha_s)\,(\alpha_{fs}-C_{fs}^{s}\alpha_s)}\right]+V_{fs}^{\mathrm{e}}. \tag{37}$$

The momentum equation for fine solid (37) has enhanced density for fine-solid in the inertial and gravity terms, but with reduced fluxes due to the entrapped fluid in it. Next, we construct similar fluid momentum equation.

2.3.3. Momentum equation for bulk fluid

We consider the following momentum equation for bulk fluid.

$$\frac{\partial}{\partial t}\,(\rho_f\bar{\alpha}_f\bar{\mathbf{u}}_f)+\nabla\cdot(\rho_f\bar{\alpha}_f\bar{\mathbf{u}}_f^2)=-\bar{\alpha}_f\nabla p+\rho_f\bar{\alpha}_f\mathbf{g}+K_{\mathrm{f}}^{\mathrm{s}}(\mathbf{u}_s-\bar{\mathbf{u}}_f) +K_{\mathrm{f}}^{\mathrm{fs}}(\bar{\mathbf{u}}_{fs}-\bar{\mathbf{u}}_f)+K_{\text{fs-es}}^{\mathrm{f}}(\mathbf{u}_{fs}^{e_s}-\bar{\mathbf{u}}_f)+V_f. \tag{38}$$

Using (21), the first term of (38) becomes

$$\frac{\partial}{\partial t}(\rho_f\bar{\alpha}_f\bar{\mathbf{u}}_f)=\frac{\partial}{\partial t}\left[\rho_f\left(\alpha_f\mathbf{u}_f-(C_f^s-C_{fs}^{s}C_f^{fs})\alpha_s\mathbf{u}_s-C_f^{fs}\alpha_{fs}\,\mathbf{u}_{fs}\right)\right]. \tag{39a}$$

Again by using (21),

$$\nabla\cdot(\rho_f\bar{\alpha}_f\bar{\mathbf{u}}_f^2)=\nabla\cdot\left[\rho_f\frac{(\alpha_f\mathbf{u}_f-(C_f^s-C_{fs}^{s}C_f^{fs})\alpha_s\mathbf{u}_s-C_f^{fs}\alpha_{fs}\,\mathbf{u}_{fs})^2}{\alpha_f-(C_f^s-C_{fs}^{s}C_f^{fs})\alpha_s-C_f^{fs}\alpha_{fs}}\right]. \tag{39b}$$

The pressure gradient term is

$$-\bar{\alpha}_f\nabla p=-\left[\alpha_f-(C_f^s-C_{fs}^{s}C_f^{fs})\alpha_s-C_f^{fs}\alpha_{fs}\right]\nabla p. \tag{39c}$$

The gravity term becomes

$$\rho_f\bar{\alpha}_f\mathbf{g}=\rho_f\left[\alpha_f-(C_f^s-C_{fs}^{s}C_f^{fs})\alpha_s-C_f^{fs}\alpha_{fs}\right]\mathbf{g}. \tag{39d}$$

Next, the drag terms are also rearranged as

$$K_{\mathrm{f}}^{\mathrm{s}}(\mathbf{u}_s-\bar{\mathbf{u}}_f)+K_{\mathrm{f}}^{\mathrm{fs}}(\bar{\mathbf{u}}_{fs}-\bar{\mathbf{u}}_f)+K_{\text{fs-es}}^{\mathrm{f}}(\mathbf{u}_{fs}^{e_s}-\bar{\mathbf{u}}_f) =-\mathcal{K}_d^2\left[\frac{\alpha_f(\mathbf{u}_f-\mathbf{u}_s)+C_f^{fs}\alpha_{fs}\,(\mathbf{u}_s-\mathbf{u}_{fs})}{(\alpha_f-C_f^{fs}\alpha_{fs}-(C_f^s-C_f^{fs}C_{fs}^{s})\alpha_s)}\right] -\mathcal{K}_d^3\left[\frac{\alpha_f\,\alpha_{fs}(\mathbf{u}_f-\mathbf{u}_{fs})-C_f^s\alpha_s\,\alpha_{fs}\,(\mathbf{u}_s-\mathbf{u}_{fs})-C_{fs}^{s}\alpha_f\alpha_s(\mathbf{u}_f-\mathbf{u}_s)}{\left(\alpha_f-C_f^{fs}\alpha_{fs}-(C_f^s-C_f^{fs}C_{fs}^{s})\alpha_s\right)\left(\alpha_{fs}-C_{fs}^{s}\alpha_s\right)}\right]. \tag{39e}$$

Using (39a)–(39e) in (38), we get the fluid momentum equation in the form:

$$\frac{\partial}{\partial t}\left[\rho_f\left(\alpha_f\mathbf{u}_f-(C_f^s-C_{fs}^{s}C_f^{fs})\alpha_s\mathbf{u}_s-C_f^{fs}\alpha_{fs}\,\mathbf{u}_{fs}\right)\right] +\nabla\cdot\left[\frac{\rho_f(\alpha_f\mathbf{u}_f-(C_f^s-C_{fs}^{s}C_f^{fs})\alpha_s\mathbf{u}_s-C_f^{fs}\alpha_{fs}\,\mathbf{u}_{fs})^2}{(\alpha_f-(C_f^s-C_{fs}^{s}C_f^{fs})\alpha_s-C_f^{fs}\alpha_{fs})}\right] =-\left[\alpha_f-(C_f^s-C_{fs}^{s}C_f^{fs})\alpha_s-C_f^{fs}\alpha_{fs}\right]\nabla p -\mathcal{K}_d^2\left[\frac{\alpha_f(\mathbf{u}_f-\mathbf{u}_s)+C_f^{fs}\alpha_{fs}\,(\mathbf{u}_s-\mathbf{u}_{fs})}{(\alpha_f-C_f^{fs}\alpha_{fs}-(C_f^s-C_f^{fs}C_{fs}^{s})\alpha_s)}\right] -\mathcal{K}_d^3\left[\frac{\alpha_f\,\alpha_{fs}(\mathbf{u}_f-\mathbf{u}_{fs})-C_f^s\alpha_s\,\alpha_{fs}\,(\mathbf{u}_s-\mathbf{u}_{fs})-C_{fs}^{s}\alpha_f\alpha_s(\mathbf{u}_f-\mathbf{u}_s)}{(\alpha_f-C_f^{fs}\alpha_{fs}-(C_f^s-C_f^{fs}C_{fs}^{s})\alpha_s)(\alpha_{fs}-C_{fs}^{s}\alpha_s)}\right] +\rho_f\left(\alpha_f-(C_f^s-C_{fs}^{s}C_f^{fs})\alpha_s-C_f^{fs}\alpha_{fs}\right)\mathbf{g}+V_f. \tag{40}$$

In (40), there is the same fluid phase density in the inertial and the gravity terms and there is no change in the viscous force term. However, importantly, the fluid fluxes are reduced due to the entrapped portion of the fluid in solid and fine-solid. This can be seen in the inertial and the gravity terms.

2.3.4. Fine-solid momentum equation without solid flux terms

Next, we want to formally remove the solid flux terms in the time derivative of (37). This allows us to obtain a more structured and usual momentum balance equation for fine-solid. This can be achieved by combining (33) and (37). For this, we multiply (33) by $C_{fs}^{s}\rho_{fs}^{e}$, (37) by ρ_s^e and add them. Then, the first terms on their left hand sides associated with local time derivatives give:

$$\rho_s^e\rho_{fs}^e\frac{\partial}{\partial t}\,\left(\alpha_{fs}\mathbf{u}_{fs}\right), \tag{41a}$$

and the second terms on their left hand sides give:

$$\rho_s^e\rho_{fs}^eC_{fs}^{s}\nabla\cdot(\alpha_s\mathbf{u}_s\mathbf{u}_s)+\rho_s^e\rho_{fs}^e\nabla\cdot\frac{(\alpha_{fs}\mathbf{u}_{fs}-C_{fs}^{s}\alpha_s\mathbf{u}_s)^2}{\alpha_{fs}-C_{fs}^{s}\alpha_s} =\rho_s^e\rho_{fs}^e\left[\nabla\cdot\alpha_{fs}\mathbf{u}_{fs}\mathbf{u}_{fs}+\nabla\cdot\frac{C_{fs}^{s}\alpha_s\alpha_{fs}}{\alpha_{fs}-C_{fs}^{s}\alpha_s}(\mathbf{u}_s-\mathbf{u}_{fs})^2\right]. \tag{41b}$$

The pressure-gradient terms in the first terms on the right hand sides of (33) and (37) sum up to:

$$-\left[C_{fs}^{s}\rho_{fs}^e\alpha_s^e+\rho_s^e(1+C_f^{fs})(\alpha_{fs}-C_{fs}^{s}\alpha_s)\right]\nabla p. \tag{41c}$$

Similarly, the second terms on the right hand sides of (33) and (37) associated with drag yield:

$$\left[\frac{\alpha_{fs}\mathcal{K}_d^1(C_{fs}^{s}\rho_{fs}^e-\rho_s^e)}{\alpha_{fs}-C_{fs}^{s}\alpha_s}-\frac{C_{fs}^{s}C_f^{fs}\alpha_{fs}\rho_{fs}^e\mathcal{K}_d^2}{\alpha_f-C_f^{fs}\alpha_{fs}-(C_f^s-C_f^{fs}C_{fs}^{s})\alpha_s} +\frac{C_f^s\,\rho_s^e\alpha_s\,\alpha_{fs}\mathcal{K}_d^3}{(\alpha_f-C_f^{fs}\alpha_{fs}-(C_f^s-C_f^{fs}C_{fs}^{s})\alpha_s)(\alpha_{fs}-C_{fs}^{s}\alpha_s)}\right](\mathbf{u}_{fs}-\mathbf{u}_s) +\left[\frac{C_{fs}^{s}\alpha_f\left[\rho_{fs}^e\mathcal{K}_d^2(\alpha_{fs}-C_{fs}^{s}\alpha_s)-\rho_s^e\alpha_s\mathcal{K}_d^3\right]}{(\alpha_f-C_f^{fs}\alpha_{fs}-(C_f^s-C_f^{fs}C_{fs}^{s})\alpha_s)(\alpha_{fs}-C_{fs}^{s}\alpha_s)}\right](\mathbf{u}_f-\mathbf{u}_s) +\frac{\rho_s^e\alpha_f\,\alpha_{fs}\mathcal{K}_d^3}{(\alpha_f-C_f^{fs}\alpha_{fs}-(C_f^s-C_f^{fs}C_{fs}^{s})\alpha_s)(\alpha_{fs}-C_{fs}^{s}\alpha_s)}(\mathbf{u}_f-\mathbf{u}_{fs}). \tag{41d}$$

The gravity terms of (33) and (37) sum to:

$$\left(\rho_s^e\rho_{fs}^eC_{fs}^{s}\alpha_s+\rho_s^e\rho_{fs}^e(\alpha_{fs}-C_{fs}^{s}\alpha_s)\right)\mathbf{g}=\rho_s^e\,\rho_{fs}^e\alpha_{fs}\mathbf{g}, \tag{41e}$$

whereas the fourth terms (i.e., viscous terms) sum to:

$$\rho_s^eV_{fs}^e+C_{fs}^{s}\rho_{fs}^eV_s^e. \tag{41f}$$

Collecting all the expressions from (41a)–(41f), we obtain the following alternative equation to (37), which does not contain the solid flux terms in the local time derivative.

$$\rho_s^e\rho_{fs}^e\left[\frac{\partial}{\partial t}\,\left(\alpha_{fs}\mathbf{u}_{fs}\right)+\nabla\cdot\alpha_{fs}\mathbf{u}_{fs}\mathbf{u}_{fs}+\nabla\cdot\frac{C_{fs}^{s}\alpha_s\alpha_{fs}}{\alpha_{fs}-C_{fs}^{s}\alpha_s}(\mathbf{u}_s-\mathbf{u}_{fs})^2\right]$$

$$
\begin{aligned}
&= -\left[C^s_{fs}\rho^e_{fs}\alpha^e_s + \rho^e_s(1+C^{fs}_f)(\alpha_{fs}-C^s_{fs}\alpha_s)\right]\nabla p\\
&+\rho^e_s\rho^e_{fs}\alpha_{fs}\mathbf{g} + \left[\frac{(C^s_{fs}\rho^e_{fs}-\rho^e_s)\,\alpha_{fs}\mathcal{K}^1_d}{\alpha_{fs}-C^s_{fs}\alpha_s} - \frac{C^s_{fs}C^{fs}_f\alpha_{fs}\,\rho^e_{fs}\mathcal{K}^2_d}{\alpha_f - C^{fs}_f\alpha_{fs} - (C^s_f - C^{fs}_f C^s_{fs})\alpha_s}\right.\\
&\left.+\frac{C^s_f\,\rho^e_s\alpha_s\,\alpha_{fs}\mathcal{K}^3_d}{(\alpha_f - C^{fs}_f\alpha_{fs} - (C^s_f - C^{fs}_f C^s_{fs})\alpha_s)(\alpha_{fs}-C^s_{fs}\alpha_s)}\right](\mathbf{u}_{fs}-\mathbf{u}_s)\\
&+\left[\frac{C^s_{fs}\alpha_f\left[\rho^e_{fs}\mathcal{K}^2_d(\alpha_{fs}-C^s_{fs}\alpha_s)-\rho^e_s\alpha_s\mathcal{K}^3_d\right]}{(\alpha_f - C^{fs}_f\alpha_{fs} - (C^s_f - C^{fs}_f C^s_{fs})\alpha_s)(\alpha_{fs}-C^s_{fs}\alpha_s)}\right](\mathbf{u}_f-\mathbf{u}_s)\\
&+\frac{\rho^e_s\alpha_f\,\alpha_{fs}\mathcal{K}^3_d}{(\alpha_f - C^{fs}_f\alpha_{fs} - (C^s_f - C^{fs}_f C^s_{fs})\alpha_s)(\alpha_{fs}-C^s_{fs}\alpha_s)}(\mathbf{u}_f-\mathbf{u}_{fs})\\
&+\rho^e_s V^e_{fs} + C^s_{fs}\rho^e_{fs}V^e_s. \qquad (42)
\end{aligned}
$$

Now, dividing by $\rho^e_s\,\rho^e_{fs}$ gives

$$
\begin{aligned}
&\frac{\partial}{\partial t}\left(\alpha_{fs}\mathbf{u}_{fs}\right) + \nabla\cdot\alpha_{fs}\mathbf{u}_{fs}\mathbf{u}_{fs} = -P_1\nabla p + \alpha_{fs}\mathbf{g} + \frac{V^e_{fs}}{\rho^e_{fs}} + C^s_{fs}\frac{V^e_s}{\rho^e_s}\\
&+I^1_1(\mathbf{u}_{fs}-\mathbf{u}_s) + I^1_2(\mathbf{u}_f-\mathbf{u}_s) + I^1_3(\mathbf{u}_f-\mathbf{u}_{fs})\\
&-\nabla\cdot\frac{C^s_{fs}\alpha_s\alpha_{fs}}{\alpha_{fs}-C^s_{fs}\alpha_s}(\mathbf{u}_s-\mathbf{u}_{fs})^2, \qquad (43)
\end{aligned}
$$

where

$$
\begin{aligned}
P_1 &= \frac{C^s_{fs}\alpha^e_s}{\rho^e_s} + \frac{1}{\rho^e_{fs}}(1+C^{fs}_f)(\alpha_{fs}-C^s_{fs}\alpha_s),\\
I^1_1 &= \frac{(C^s_{fs}\rho^e_{fs}-\rho^e_s)\alpha_{fs}\mathcal{K}^1_d}{\rho^e_s\,\rho^e_{fs}(\alpha_{fs}-C^s_{fs}\alpha_s)} - \frac{C^s_{fs}C^{fs}_f\alpha_{fs}\mathcal{K}^2_d}{\rho^e_s[\alpha_f - C^{fs}_f\alpha_{fs} - (C^s_f - C^{fs}_f C^s_{fs})\alpha_s]}\\
&\quad+\frac{C^s_f\alpha_s\,\alpha_{fs}\mathcal{K}^3_d}{\rho^e_{fs}(\alpha_f - C^{fs}_f\alpha_{fs} - (C^s_f - C^{fs}_f C^s_{fs})\alpha_s)(\alpha_{fs}-C^s_{fs}\alpha_s)},\\
I^1_2 &= \frac{C^s_{fs}\alpha_f\left[\rho^e_{fs}\mathcal{K}^2_d(\alpha_{fs}-C^s_{fs}\alpha_s)-\rho^e_s\alpha_s\mathcal{K}^3_d\right]}{\rho^e_s\,\rho^e_{fs}(\alpha_f - C^{fs}_f\alpha_{fs} - (C^s_f - C^{fs}_f C^s_{fs})\alpha_s)(\alpha_{fs}-C^s_{fs}\alpha_s)},\\
I^1_3 &= \frac{\alpha_f\,\alpha_{fs}\mathcal{K}^3_d}{\rho^e_{fs}(\alpha_f - C^{fs}_f\alpha_{fs} - (C^s_f - C^{fs}_f C^s_{fs})\alpha_s)(\alpha_{fs}-C^s_{fs}\alpha_s)}. \qquad (44)
\end{aligned}
$$

For the generalized momentum equation for fine-solid, we again multiply (43) by ρ^e_{fs} ($= \rho_{fs} + C^{fs}_f\rho_f$ is a constant for density preserving materials if variation in C^{fs}_f is negligible), and obtain:

$$
\begin{aligned}
&\frac{\partial}{\partial t}\left(\rho^e_{fs}\alpha_{fs}\mathbf{u}_{fs}\right) + \nabla\cdot\rho^e_{fs}\alpha_{fs}\mathbf{u}_{fs}\mathbf{u}_{fs} = -\rho^e_{fs}P_1\nabla p + \alpha_{fs}\rho^e_{fs}\mathbf{g} + V^e_{fs}\\
&+C^s_{fs}\frac{\rho^e_{fs}V^e_s}{\rho^e_s} + \rho^e_{fs}I^1_1(\mathbf{u}_{fs}-\mathbf{u}_s) + \rho^e_{fs}I^1_2(\mathbf{u}_f-\mathbf{u}_s) + \rho^e_{fs}I^1_3(\mathbf{u}_f-\mathbf{u}_{fs})\\
&-\nabla\cdot\frac{\rho^e_{fs}C^s_{fs}\alpha_s\alpha_{fs}}{\alpha_{fs}-C^s_{fs}\alpha_s}(\mathbf{u}_s-\mathbf{u}_{fs})^2. \qquad (45)
\end{aligned}
$$

2.3.5. Mechanical properties of the generalized fine-solid momentum equation

The very interesting point is that in (45), left hand side (the inertial part) remains unchanged, except for the enhanced density ρ^e_{fs}. However, due to the entrapments of the weaker (fluid-type) materials into the stronger (solid-type) materials, all the terms except the body force have been changed (or, enhanced) accordingly. To explicitly highlight all the new mechanical aspects, below, we analyze all such forcing terms.

Pressure Gradients ($-\rho^e_{fs}P_1\nabla p$) : P_1 includes the effects of fine-solid entrapped in solid via C^s_{fs} and the fluid entrapped in fine-solid via C^{fs}_f. Depending on the volume fractions of fine-solid and solid, and how much fine-solid is entrapped in solid, the second term in P_1 can be positive or negative and thus enhances or reduces the pressure. If no fine-solid was entrapped in solid, the coefficient of ∇p reduces to

$$\rho^e_{fs}P_1 = (1+C^{fs}_f)\alpha_{fs}.$$

So, both volume fraction and the density of fine-solid are enhanced by the entrapped fluid in fine-solid. Furthermore, if no fluid is entrapped in fine-solid, then $\rho^e_{fs}P_1 = \alpha_{fs}$, which is the usual pressure factor.

Probably, the most important aspect of (45) is the appearance of the advection like term, $\nabla\cdot\frac{\rho^e_{fs}C^s_{fs}\alpha_s\alpha_{fs}}{\alpha_{fs}-C^s_{fs}\alpha_s}(\mathbf{u}_s-\mathbf{u}_{fs})^2$ together with the pressure gradient term $-\rho^e_{fs}P_1\nabla p$ those eventually will generate the composite virtual mass force structure. This will be clear in the following section. If there is no entrapment, the advection like term disappears and $\rho^e_{fs}P_1$ is the only fine-solid volume fraction factor in pressure gradient.

Drag Forces: There are three drag force components, each having its own composite drag coefficients. If all the entrapments are ignored, then $I^1_1 = -\mathcal{K}^1_d/\rho_{fs} = K^{\mathrm{fs}}_{\mathrm{s}}/\rho_{fs}$. But, $I^1_2 = 0$ as it is originated from interactions between fluid and solid that does not involve fine-solid, whereas $I^1_3 = \mathcal{K}^3_d/\rho_{fs} = K^{\mathrm{fs}}_{\mathrm{f}}/\rho_{fs}$. In this case, the net drag force in the fine-solid momentum equation will be $K^{\mathrm{fs}}_{\mathrm{s}}(\mathbf{u}_{fs}-\mathbf{u}_s) + K^{\mathrm{fs}}_{\mathrm{f}}(\mathbf{u}_f-\mathbf{u}_{fs})$, which is the usual drag force for fine-solid in the three-phase debris flow.

Viscous Forces: In (45), the viscous forces appear in the expression $V^e_{fs} + C^s_{fs}\frac{\rho^e_{fs}V^e_s}{\rho^e_s}$. If all the entrapments are ignored, the only effective viscous force is due to $V^e_{fs} = V_{fs}$, the original viscous force for fine-solid.

The generalized solid, fluid and fine-solid momentum equations are respectively given by (33), (40), and (45).

2.4. Momentum equations with phase densities

In the previous section, the enhanced densities were involved in the momentum equations for solid and fine-solid due to the entrapped fluid-type materials. Next, we proceed further to obtain the momentum equations in usual form with phase densities. For the sake of simplicity, (33) is divided by ρ^e_s to write in the form:

$$\frac{\partial}{\partial t}(\alpha_s\,\mathbf{u}_s) + \nabla\cdot(\alpha_s\mathbf{u}_s\mathbf{u}_s) = -\frac{\alpha^e_s}{\rho^e_s}\nabla p + \alpha_s\mathbf{g} + \frac{V^e_s}{\rho^e_s} + I^2_1(\mathbf{u}_{fs}-\mathbf{u}_s) + I^2_2(\mathbf{u}_f-\mathbf{u}_s), \qquad (46)$$

where

$$
\begin{aligned}
I^2_1 &= \frac{1}{\rho^e_s}\left[\frac{\alpha_{fs}\mathcal{K}^1_d}{\alpha_{fs}-C^s_{fs}\alpha_s} - \frac{C^{fs}_f\alpha_{fs}\mathcal{K}^2_d}{(\alpha_f - C^{fs}_f\alpha_{fs} - (C^s_f - C^{fs}_f C^s_{fs})\alpha_s)}\right],\\
I^2_2 &= \frac{\alpha_f\mathcal{K}^2_d}{\rho^e_s(\alpha_f - C^{fs}_f\alpha_{fs} - (C^s_f - C^{fs}_f C^s_{fs})\alpha_s)}. \qquad (47)
\end{aligned}
$$

Multiplying (43) by α_s, (46) by α_{fs} and then their subtraction gives the following equation with no gravity term.

$$
\begin{aligned}
0 &= -\nabla p + \frac{\rho^e_s\alpha_{fs}}{\rho^e_s\alpha_s P_1 - \alpha_{fs}\alpha^e_s}\left[\frac{\partial}{\partial t}(\alpha_s\,\mathbf{u}_s) - \frac{\alpha_s}{\alpha_{fs}}\frac{\partial}{\partial t}\left(\alpha_{fs}\mathbf{u}_{fs}\right) + \nabla\cdot(\alpha_s\mathbf{u}_s\mathbf{u}_s)\right.\\
&\quad\left.-\frac{\alpha_s}{\alpha_{fs}}\nabla\cdot\alpha_{fs}\mathbf{u}_{fs}\mathbf{u}_{fs}\right] + \frac{\rho^e_s(\alpha_s I^1_1 - \alpha_{fs}I^2_1)}{\rho^e_s\alpha_s P_1 - \alpha_{fs}\alpha^e_s}(\mathbf{u}_{fs}-\mathbf{u}_s)\\
&\quad+\frac{\rho^e_s(\alpha_s I^1_2 - \alpha_{fs}I^2_2)}{\rho^e_s\alpha_s P_1 - \alpha_{fs}\alpha^e_s}(\mathbf{u}_f-\mathbf{u}_s) + \frac{\rho^e_s\alpha_s I^1_3}{\rho^e_s\alpha_s P_1 - \alpha_{fs}\alpha^e_s}(\mathbf{u}_f-\mathbf{u}_{fs})\\
&\quad+\frac{\rho^e_s\alpha_s}{\rho^e_s\alpha_s P_1 - \alpha_{fs}\alpha^e_s}\nabla\cdot\frac{C^s_{fs}\alpha_s\alpha_{fs}}{\alpha_{fs}-C^s_{fs}\alpha_s}(\mathbf{u}_s-\mathbf{u}_{fs})^2\\
&\quad+\frac{1}{\rho^e_{fs}(\rho^e_s\alpha_s P_1 - \alpha_{fs}\alpha^e_s)}\left(\rho^e_s\alpha_s V^e_{fs} + C^s_{fs}\alpha_s\rho^e_{fs}V^e_s - \rho^e_{fs}\alpha_{fs}V^e_s\right). \qquad (48)
\end{aligned}
$$

Next, we multiply (48) by $(\alpha_{fs}/\rho_{fs} - P_1)$ and add it with (43). We also use the mass balance Eqs. (8) and (15) to remove the time derivatives of the volume fractions of the solid and fine-solid contained in the

second terms of the right hand side of (48). The resulting equation after rearranging the terms will be

$$\begin{aligned}
&\rho_{fs}\left[\frac{\partial}{\partial t}\left(\alpha_{fs}\mathbf{u}_{fs}\right)+\nabla\cdot\alpha_{fs}\mathbf{u}_{fs}\mathbf{u}_{fs}\right]-\frac{\rho_s^e\alpha_{fs}(\alpha_{fs}-\rho_{fs}P_1)}{\rho_s^e\alpha_s P_1-\alpha_{fs}\alpha_s^e}\left(\frac{\partial\mathbf{u}_s}{\partial t}-\frac{\partial\mathbf{u}_{fs}}{\partial t}\right)\\
&=\ -\alpha_{fs}\nabla p+I_1^3(\mathbf{u}_{fs}-\mathbf{u}_s)+I_2^3(\mathbf{u}_f-\mathbf{u}_s)+I_3^3(\mathbf{u}_f-\mathbf{u}_{fs})+\rho_{fs}\alpha_{fs}\mathbf{g}\\
&+\ \frac{(\alpha_{fs}-\rho_{fs}P_1)}{\rho_{fs}^e(\rho_s^e\alpha_s P_1-\alpha_{fs}\alpha_s^e)}\left(\rho_s^e\alpha_s V_{fs}^e+C_{fs}^s\alpha_s\rho_{fs}^e V_s^e-\rho_{fs}^e\alpha_{fs}V_s^e\right)\\
&+\ \frac{\rho_{fs}V_{fs}^e}{\rho_{fs}^e}+\frac{\rho_{fs}}{\rho_s^e}C_{fs}^s V_s^e+\frac{\alpha_{fs}(\rho_s^e\alpha_s-\rho_{fs}\alpha_s^e)}{\rho_s^e\alpha_s P_1-\alpha_{fs}\alpha_s^e}\nabla\cdot\frac{C_{fs}^s\alpha_s\alpha_{fs}}{\alpha_{fs}-C_{fs}^s\alpha_s}(\mathbf{u}_s-\mathbf{u}_{fs})^2\\
&+\ \frac{\rho_s^e\alpha_{fs}(\alpha_{fs}-\rho_{fs}P_1)}{\rho_s^e\alpha_s P_1-\alpha_{fs}\alpha_s^e}\left(\mathbf{u}_s\cdot\nabla\mathbf{u}_s-\mathbf{u}_{fs}\cdot\nabla\mathbf{u}_{fs}\right),
\end{aligned}\tag{49}$$

where

$$\begin{aligned}
I_1^3&=\frac{\rho_s^e(\alpha_s I_1^1-\alpha_{fs}I_1^2)(\alpha_{fs}-\rho_{fs}P_1)}{\rho_s^e\alpha_s P_1-\alpha_{fs}\alpha_s^e}+\rho_{fs}I_1^1,\\
I_2^3&=\frac{\rho_s^e(\alpha_s I_2^1-\alpha_{fs}I_2^2)(\alpha_{fs}-\rho_{fs}P_1)}{\rho_s^e\alpha_s P_1-\alpha_{fs}\alpha_s^e}+\rho_{fs}I_2^1,\\
I_3^3&=\frac{\rho_s^e\alpha_s(\alpha_{fs}-\rho_{fs}P_1)I_3^1}{\rho_s^e\alpha_s P_1-\alpha_{fs}\alpha_s^e}+\rho_{fs}I_3^1.
\end{aligned}\tag{50}$$

The last term on the right hand side of (49) can be combined with the second term of the left hand side so that the resulting momentum equation for fine-solid becomes

$$\begin{aligned}
&\rho_{fs}\left[\frac{\partial}{\partial t}\left(\alpha_{fs}\mathbf{u}_{fs}\right)+\nabla\cdot\alpha_{fs}\mathbf{u}_{fs}\mathbf{u}_{fs}\right]=-\alpha_{fs}\nabla p+I_1^3(\mathbf{u}_{fs}-\mathbf{u}_s)\\
&+I_2^3(\mathbf{u}_f-\mathbf{u}_s)+I_3^3(\mathbf{u}_f-\mathbf{u}_{fs})+\rho_{fs}\alpha_{fs}\mathbf{g}\\
&+\frac{\alpha_{fs}-\rho_{fs}P_1}{\rho_{fs}^e(\rho_s^e\alpha_s P_1-\alpha_{fs}\alpha_s^e)}\left(\rho_s^e\alpha_s V_{fs}^e+C_{fs}^s\alpha_s\rho_{fs}^e V_s^e-\rho_{fs}^e\alpha_{fs}V_s^e\right)\\
&+\frac{\rho_{fs}V_{fs}^e}{\rho_{fs}^e}+\frac{\rho_{fs}}{\rho_s^e}C_{fs}^s V_s^e-\frac{\rho_s^e\alpha_s(\alpha_{fs}-\rho_{fs}P_1)}{\rho_s^e\alpha_s P_1-\alpha_{fs}\alpha_s^e}\nabla\cdot\frac{C_{fs}^s\alpha_s\alpha_{fs}}{\alpha_{fs}-C_{fs}^s\alpha_s}(\mathbf{u}_s-\mathbf{u}_{fs})^2\\
&+\frac{\rho_s^e\alpha_s\alpha_{fs}(\alpha_{fs}-\rho_{fs}P_1)}{\rho_s^e\alpha_s P_1-\alpha_{fs}\alpha_s^e}\left(\frac{d\mathbf{u}_s}{dt}-\frac{d\mathbf{u}_{fs}}{dt}\right).
\end{aligned}\tag{51}$$

Multiplying (48) by $\left(\frac{\alpha_s}{\rho_s}-\frac{\alpha_s^e}{\rho_s^e}\right)$ and adding with (46), we get the similar solid momentum equation:

$$\begin{aligned}
&\rho_s\left[\frac{\partial}{\partial t}(\alpha_s\mathbf{u}_s)+\nabla\cdot(\alpha_s\mathbf{u}_s\mathbf{u}_s)\right]=-\alpha_s\nabla p+\rho_s\alpha_s\mathbf{g}+I_1^4(\mathbf{u}_{fs}-\mathbf{u}_s)\\
&+I_2^4(\mathbf{u}_f-\mathbf{u}_s)+I_3^4(\mathbf{u}_f-\mathbf{u}_{fs})\\
&+\frac{(\alpha_s\rho_s^e-\alpha_s^e\rho_s)}{\rho_s^e\rho_{fs}^e(\rho_s^e\alpha_s P_1-\alpha_{fs}\alpha_s^e)}\left(\rho_s^e\alpha_s V_{fs}^e+C_{fs}^s\alpha_s\rho_{fs}^e V_s^e-\rho_{fs}^e\alpha_{fs}V_s^e\right)\\
&+V_s^e\frac{\rho_s}{\rho_s^e}+\frac{\alpha_s(\alpha_s\rho_s^e-\alpha_s^e\rho_s)}{(\rho_s^e\alpha_s P_1-\alpha_{fs}\alpha_s^e)}\nabla\cdot\frac{C_{fs}^s\alpha_s\alpha_{fs}}{\alpha_{fs}-C_{fs}^s\alpha_s}(\mathbf{u}_{fs}-\mathbf{u}_s)^2\\
&+\frac{\alpha_s\alpha_{fs}(\alpha_s\rho_s^e-\alpha_s^e\rho_s)}{(\rho_s^e\alpha_s P_1-\alpha_{fs}\alpha_s^e)}\left(\frac{d\mathbf{u}_s}{dt}-\frac{d\mathbf{u}_{fs}}{dt}\right),
\end{aligned}\tag{52}$$

where

$$\begin{aligned}
I_1^4&=\frac{(\alpha_s\rho_s^e-\alpha_s^e\rho_s)(\alpha_s I_1^1-\alpha_{fs}I_1^2)}{\rho_s^e\alpha_s P_1-\alpha_{fs}\alpha_s^e}+\rho_s I_1^2,\\
I_2^4&=\frac{(\alpha_s\rho_s^e-\alpha_s^e\rho_s)(\alpha_s I_2^1-\alpha_{fs}I_2^2)}{\rho_s^e\alpha_s P_1-\alpha_{fs}\alpha_s^e}+\rho_s I_2^2,\\
I_3^4&=\frac{I_3^1(\alpha_s\rho_s^e-\alpha_s^e\rho_s)}{\rho_s^e\alpha_s P_1-\alpha_{fs}\alpha_s^e}.
\end{aligned}$$

Again, (40) is written as

$$\begin{aligned}
&\frac{\partial}{\partial t}\left[(\alpha_f\mathbf{u}_f-(C_f^s-C_{fs}^sC_f^{fs})\alpha_s\mathbf{u}_s-C_f^{fs}\alpha_{fs}\mathbf{u}_{fs})\right]\\
&\quad+\nabla\cdot\left[\frac{(\alpha_f\mathbf{u}_f-(C_f^s-C_{fs}^sC_f^{fs})\alpha_s\mathbf{u}_s-C_f^{fs}\alpha_{fs}\mathbf{u}_{fs})^2}{(\alpha_f-(C_f^s-C_{fs}^sC_f^{fs})\alpha_s-C_f^{fs}\alpha_{fs})}\right]\\
&=-P_2\nabla p+I_1^5(\mathbf{u}_{fs}-\mathbf{u}_s)+I_2^5(\mathbf{u}_f-\mathbf{u}_s)+I_3^5(\mathbf{u}_f-\mathbf{u}_{fs})\\
&\quad+(\alpha_f-(C_f^s-C_{fs}^sC_f^{fs})\alpha_s-C_f^{fs}\alpha_{fs})\mathbf{g}+V_f,
\end{aligned}\tag{53}$$

where

$$\begin{aligned}
P_2&=\frac{1}{\rho_f}(\alpha_f-(C_f^s-C_{fs}^sC_f^{fs})\alpha_s-C_f^{fs}\alpha_{fs}),\\
I_1^5&=\frac{\alpha_{fs}(C_f^{fs}\mathcal{K}_d^2(\alpha_{fs}-C_{fs}^s\alpha_s)+\alpha_f\mathcal{K}_d^3)}{(\alpha_f-C_f^{fs}\alpha_{fs}-(C_f^s-C_f^{fs}C_{fs}^s)\alpha_s)(\alpha_{fs}-C_{fs}^s\alpha_s)},\\
I_2^5&=\frac{\alpha_f(\mathcal{K}_d^2(\alpha_{fs}-C_{fs}^s\alpha_s)+C_{fs}^s\alpha_s\mathcal{K}_d^3)}{(\alpha_f-C_f^{fs}\alpha_{fs}-(C_f^s-C_f^{fs}C_{fs}^s)\alpha_s)(\alpha_{fs}-C_{fs}^s\alpha_s)},\\
I_3^5&=-\frac{C_f^s\alpha_s\alpha_{fs}\mathcal{K}_d^3}{(\alpha_f-C_f^{fs}\alpha_{fs}-(C_f^s-C_f^{fs}C_{fs}^s)\alpha_s)(\alpha_{fs}-C_{fs}^s\alpha_s)}.
\end{aligned}$$

For the fluid momentum equation with phase density, we again multiply (53) by ρ_f to obtain:

$$\begin{aligned}
&\frac{\partial}{\partial t}\rho_f\left[(\alpha_f\mathbf{u}_f-(C_f^s-C_{fs}^sC_f^{fs})\alpha_s\mathbf{u}_s-C_f^{fs}\alpha_{fs}\mathbf{u}_{fs})\right]\\
&\quad+\nabla\cdot\rho_f\left[\frac{(\alpha_f\mathbf{u}_f-(C_f^s-C_{fs}^sC_f^{fs})\alpha_s\mathbf{u}_s-C_f^{fs}\alpha_{fs}\mathbf{u}_{fs})^2}{(\alpha_f-(C_f^s-C_{fs}^sC_f^{fs})\alpha_s-C_f^{fs}\alpha_{fs})}\right]\\
&=-\rho_f P_2\nabla p+\rho_f I_1^5(\mathbf{u}_{fs}-\mathbf{u}_s)+\rho_f I_2^5(\mathbf{u}_f-\mathbf{u}_s)+\rho_f I_3^5(\mathbf{u}_f-\mathbf{u}_{fs})\\
&\quad+\rho_f(\alpha_f-(C_f^s-C_{fs}^sC_f^{fs})\alpha_s-C_f^{fs}\alpha_{fs})\mathbf{g}+\rho_f V_f.
\end{aligned}\tag{54}$$

Thus, (52), (51), and (54) are respectively the intermediate momentum equations for solid, fine-solid and fluid. Next, we employ these equations to construct the momentum equation with virtual mass forces.

3. Momentum equations with virtual mass forces

In this section, we derive the momentum equations for the three phases with explicit evolution of virtual mass terms.

3.1. Momentum equation for fluid

We use (43) and (46) in (53) and rearrange the terms to get

$$\begin{aligned}
&\frac{\partial}{\partial t}(\alpha_f\mathbf{u}_f)+\nabla\cdot(\alpha_f\mathbf{u}_f\mathbf{u}_f)=-P_3\nabla p+\alpha_f\mathbf{g}+I_1^6(\mathbf{u}_{fs}-\mathbf{u}_s)+I_2^6(\mathbf{u}_f-\mathbf{u}_s)\\
&+I_3^6(\mathbf{u}_f-\mathbf{u}_{fs})-\Big[(C_f^s-C_{fs}^sC_f^{fs})\nabla\cdot(\alpha_s\mathbf{u}_s\mathbf{u}_s)+C_f^{fs}\nabla\cdot\alpha_{fs}\mathbf{u}_{fs}\mathbf{u}_{fs}\\
&-\nabla\cdot(\alpha_f\mathbf{u}_f\mathbf{u}_f)-\nabla\cdot\frac{C_{fs}^s\alpha_s\alpha_{fs}}{\alpha_{fs}-C_{fs}^s\alpha_s}(\mathbf{u}_s-\mathbf{u}_{fs})^2\\
&+\nabla\cdot\left(\frac{(\alpha_f\mathbf{u}_f-(C_f^s-C_{fs}^sC_f^{fs})\alpha_s\mathbf{u}_s-C_f^{fs}\alpha_{fs}\mathbf{u}_{fs})^2}{(\alpha_f-(C_f^s-C_{fs}^sC_f^{fs})\alpha_s-C_f^{fs}\alpha_{fs})}\right)\Big]+V_f^1,
\end{aligned}\tag{55}$$

where

$$\begin{aligned}
P_3&=C_f^{fs}P_1+(C_f^s-C_{fs}^sC_f^{fs})\frac{\alpha_s^e}{\rho_s^e}+P_2,\\
I_1^6&=(C_f^s-C_{fs}^sC_f^{fs})I_1^2+C_f^{fs}I_1^1+I_1^5,\\
I_2^6&=(C_f^s-C_{fs}^sC_f^{fs})I_2^2+C_f^{fs}I_2^1+I_2^5,\\
I_3^6&=C_f^{fs}I_3^1+I_3^5,\\
V_f^1&=\left(C_f^s-C_{fs}^sC_f^{fs}\right)\frac{V_s^e}{\rho_s^e}+C_f^{fs}\left(\frac{V_{fs}^e}{\rho_{fs}^e}+C_{fs}^s\frac{V_s^e}{\rho_s^e}\right)+V_f\Big).
\end{aligned}$$

Next, we multiply (43) by α_f, (55) by α_{fs} and then subtract them so as to eliminate the gravity term:

$$\begin{aligned}
0=&-\nabla p+\frac{\alpha_{fs}}{\alpha_f P_1-\alpha_{fs}P_3}\left[\frac{\partial}{\partial t}(\alpha_f\mathbf{u}_f)-\frac{\alpha_f}{\alpha_{fs}}\frac{\partial}{\partial t}\left(\alpha_{fs}\mathbf{u}_{fs}\right)\right.\\
&\left.+\nabla\cdot(\alpha_f\mathbf{u}_f\mathbf{u}_f)-\frac{\alpha_f}{\alpha_{fs}}\nabla\cdot\alpha_{fs}\mathbf{u}_{fs}\mathbf{u}_{fs}\right]\\
&-\frac{1}{\alpha_f P_1-\alpha_{fs}P_3}\left[(\alpha_{fs}I_1^6-\alpha_f I_1^1)(\mathbf{u}_{fs}-\mathbf{u}_s)+(\alpha_{fs}I_2^6-\alpha_f I_2^1)(\mathbf{u}_f-\mathbf{u}_s)\right.
\end{aligned}$$

$$
\begin{aligned}
&+(\alpha_{fs} I_3^6 - \alpha_f I_3^1)(\mathbf{u}_f - \mathbf{u}_{fs})\big] \\
&- \frac{1}{\alpha_f P_1 - \alpha_{fs} P_3}\left(\alpha_{fs} V_f^1 - \alpha_f\left(\frac{V_{fs}^e}{\rho_{fs}^e} + C_{fs}^s \frac{V_s^e}{\rho_s^e}\right)\right) \\
&+ \frac{1}{\alpha_f P_1 - \alpha_{fs} P_3}\Bigg[\alpha_{fs}(C_f^s - C_{fs}^s C_f^{fs})\nabla\cdot(\alpha_s \mathbf{u}_s \mathbf{u}_s) + C_f^{fs}\alpha_{fs}\nabla\cdot\alpha_{fs}\mathbf{u}_{fs}\mathbf{u}_{fs} \\
&-\alpha_{fs}\nabla\cdot(\alpha_f \mathbf{u}_f \mathbf{u}_f) - \alpha_{fs}\nabla\cdot\frac{C_{fs}^s \alpha_s \alpha_{fs}}{\alpha_{fs} - C_{fs}^s \alpha_s}(\mathbf{u}_s - \mathbf{u}_{fs})^2 \\
&+\alpha_{fs}\nabla\cdot\left(\frac{(\alpha_f \mathbf{u}_f - (C_f^s - C_{fs}^s C_f^{fs})\alpha_s \mathbf{u}_s - C_f^{fs}\alpha_{fs}\mathbf{u}_{fs})^2}{\alpha_f - (C_f^s - C_{fs}^s C_f^{fs})\alpha_s - C_f^{fs}\alpha_{fs}}\right) \\
&-\alpha_f \nabla\cdot\frac{C_{fs}^s \alpha_s \alpha_{fs}}{\alpha_{fs} - C_{fs}^s \alpha_s}(\mathbf{u}_s - \mathbf{u}_{fs})^2\Bigg]\cdot
\end{aligned}
\tag{56}
$$

Similarly, the gravity terms are eliminated when we multiply (46) by α_f, (55) by α_s and then subtract:

$$
\begin{aligned}
0 = &-\nabla p + \frac{\rho_s^e \alpha_s}{\alpha_f \alpha_s^e - \rho_s^e \alpha_s P_3}\left[\frac{\partial}{\partial t}(\alpha_f \mathbf{u}_f) - \frac{\alpha_f}{\alpha_s}\frac{\partial}{\partial t}(\alpha_s \mathbf{u}_s) + \nabla\cdot(\alpha_f \mathbf{u}_f \mathbf{u}_f)\right. \\
&\left.-\frac{\alpha_f}{\alpha_s}\nabla\cdot\alpha_s \mathbf{u}_s \mathbf{u}_s\right] - \frac{\rho_s^e}{\alpha_f \alpha_s^e - \rho_s^e \alpha_s P_3}\left[(\alpha_s I_1^6 - \alpha_f I_1^2)(\mathbf{u}_{fs} - \mathbf{u}_s)\right. \\
&\left.+(\alpha_s I_2^6 - \alpha_f I_2^2)(\mathbf{u}_f - \mathbf{u}_s) + \alpha_s I_3^6(\mathbf{u}_f - \mathbf{u}_{fs})\right] \\
&- \frac{\rho_s^e}{\alpha_f \alpha_s^e - \rho_s^e \alpha_s P_3}\left(\alpha_s V_f^1 - \alpha_f \frac{V_s^e}{\rho_s^e}\right) \\
&+ \frac{\rho_s^e \alpha_s}{\alpha_f \alpha_s^e - \rho_s^e \alpha_s P_3}\Bigg[(C_f^s - C_{fs}^s C_f^{fs})\nabla\cdot(\alpha_s \mathbf{u}_s \mathbf{u}_s) \\
&+ C_f^{fs}\nabla\cdot\alpha_{fs}\mathbf{u}_{fs}\mathbf{u}_{fs} - \nabla\cdot(\alpha_f \mathbf{u}_f \mathbf{u}_f) - \nabla\cdot\frac{C_{fs}^s \alpha_s \alpha_{fs}}{\alpha_{fs} - C_{fs}^s \alpha_s}(\mathbf{u}_s - \mathbf{u}_{fs})^2 \\
&+\nabla\cdot\left(\frac{(\alpha_f \mathbf{u}_f - (C_f^s - C_{fs}^s C_f^{fs})\alpha_s \mathbf{u}_s - C_f^{fs}\alpha_{fs}\mathbf{u}_{fs})^2}{(\alpha_f - (C_f^s - C_{fs}^s C_f^{fs})\alpha_s - C_f^{fs}\alpha_{fs})}\right)\Bigg].
\end{aligned}
\tag{57}
$$

Now, we add (56) and (57) so that the following equation has the explicit appearance of the virtual mass forces due to the relative acceleration of the fluid phase with both solid and fine-solid phases, which is very much relevant for three-phase mass flow.

$$
\begin{aligned}
0 = &-2\nabla p + \frac{\alpha_f \alpha_{fs}}{(\alpha_f P_1 - \alpha_{fs} P_3)}\left(\frac{d\mathbf{u}_f}{dt} - \frac{d\mathbf{u}_{fs}}{dt}\right) \\
&+\frac{\rho_s^e \alpha_s \alpha_f}{(\alpha_f \alpha_s^e - \rho_s^e \alpha_s P_3)}\left(\frac{d\mathbf{u}_f}{dt} - \frac{d\mathbf{u}_s}{dt}\right) \\
&+ I_1^7(\mathbf{u}_{fs} - \mathbf{u}_s) + I_2^7(\mathbf{u}_f - \mathbf{u}_s) + I_3^7(\mathbf{u}_f - \mathbf{u}_{fs}) + V_f^2 \\
&-\left(\frac{\alpha_{fs}}{(\alpha_f P_1 - \alpha_{fs} P_3)} + \frac{\rho_s^e \alpha_s}{(\alpha_f \alpha_s^e - \rho_s^e \alpha_s P_3)}\right)\Big[(C_f^s - C_{fs}^s C_f^{fs})\nabla\cdot(\alpha_s \mathbf{u}_s \mathbf{u}_s) \\
&+C_f^{fs}\nabla\cdot\alpha_{fs}\mathbf{u}_{fs}\mathbf{u}_{fs} - \nabla\cdot(\alpha_f \mathbf{u}_f \mathbf{u}_f) + \nabla\cdot\frac{C_{fs}^s \alpha_s \alpha_{fs}}{\alpha_{fs} - C_{fs}^s \alpha_s}(\mathbf{u}_s - \mathbf{u}_{fs})^2 \\
&+\nabla\cdot\left(\frac{(\alpha_f \mathbf{u}_f - (C_f^s - C_{fs}^s C_f^{fs})\alpha_s \mathbf{u}_s - C_f^{fs}\alpha_{fs}\mathbf{u}_{fs})^2}{(\alpha_f - (C_f^s - C_{fs}^s C_f^{fs})\alpha_s - C_f^{fs}\alpha_{fs})}\right)\Big] \\
&-\left(\frac{\alpha_f}{(\alpha_f P_1 - \alpha_{fs} P_3)}\nabla\cdot\frac{C_{fs}^s \alpha_s \alpha_{fs}}{\alpha_{fs} - C_{fs}^s \alpha_s}(\mathbf{u}_s - \mathbf{u}_{fs})^2\right),
\end{aligned}
\tag{58}
$$

where

$$
\begin{aligned}
I_1^7 &= -\left(\frac{\alpha_{fs} I_1^6 - \alpha_f I_1^1}{\alpha_f P_1 - \alpha_{fs} P_3} + \frac{\rho_s^e(\alpha_s I_1^6 - \alpha_f I_1^2)}{\alpha_f \alpha_s^e - \rho_s^e \alpha_s P_3}\right), \\
I_2^7 &= -\left(\frac{\alpha_{fs} I_2^6 - \alpha_f I_2^1}{\alpha_f P_1 - \alpha_{fs} P_3} + \frac{\rho_s^e(\alpha_s I_2^6 - \alpha_f I_2^2)}{\alpha_f \alpha_s^e - \rho_s^e \alpha_s P_3}\right), \\
I_3^7 &= -\left(\frac{\alpha_{fs} I_3^6 - \alpha_f I_3^1}{\alpha_f P_1 - \alpha_{fs} P_3} + \frac{\rho_s^e \alpha_s I_3^6}{\alpha_f \alpha_s^e - \rho_s^e \alpha_s P_3}\right), \\
V_f^2 &= -\frac{1}{\alpha_f P_1 - \alpha_{fs} P_3}\left(\alpha_{fs} V_f^1 - \alpha_f\left(\frac{V_{fs}^e}{\rho_{fs}^e} + C_{fs}^s \frac{V_s^e}{\rho_s^e}\right)\right)
\end{aligned}
$$

$$
-\frac{\rho_s^e}{\alpha_f \alpha_s^e - \rho_s^e \alpha_s P_3}\left(\alpha_s V_f^1 - \alpha_f \frac{V_s^e}{\rho_s^e}\right)\cdot
$$

Multiplying (58) by $\left(\frac{\alpha_f}{2\rho_f} - \frac{P_3}{2}\right)$ and adding it with (55), we get the following **momentum equation for fluid with virtual mass forces.**

$$
\begin{aligned}
&\rho_f\left(\frac{\partial}{\partial t}(\alpha_f \mathbf{u}_f) + \nabla\cdot(\alpha_f \mathbf{u}_f \mathbf{u}_f)\right) = -\alpha_f \nabla p + \rho_f \alpha_f \mathbf{g} \\
&+\frac{\alpha_f \alpha_{fs}(\alpha_f - \rho_f P_3)}{2(\alpha_f P_1 - \alpha_{fs} P_3)}\left(\frac{d\mathbf{u}_f}{dt} - \frac{d\mathbf{u}_{fs}}{dt}\right) \\
&+\frac{\rho_s^e \alpha_s \alpha_f(\alpha_f - \rho_f P_3)}{2(\alpha_f \alpha_s^e - \rho_s^e \alpha_s P_3)}\left(\frac{d\mathbf{u}_f}{dt} - \frac{d\mathbf{u}_s}{dt}\right) + I_1^8(\mathbf{u}_{fs} - \mathbf{u}_s) + I_2^8(\mathbf{u}_f - \mathbf{u}_s) \\
&+I_3^8(\mathbf{u}_f - \mathbf{u}_{fs}) + \mathcal{V}_f \\
&-\left(\frac{\alpha_{fs}(\alpha_f - \rho_f P_3)}{2(\alpha_f P_1 - \alpha_{fs} P_3)} + \frac{\rho_s^e \alpha_s(\alpha_f - \rho_f P_3)}{2(\alpha_f \alpha_s^e - \rho_s^e \alpha_s P_3)} + \rho_f\right) \\
&\times\Bigg[(C_f^s - C_{fs}^s C_f^{fs})\nabla\cdot(\alpha_s \mathbf{u}_s \mathbf{u}_s) + C_f^{fs}\nabla\cdot\alpha_{fs}\mathbf{u}_{fs}\mathbf{u}_{fs} \\
&-\nabla\cdot(\alpha_f \mathbf{u}_f \mathbf{u}_f) + \nabla\cdot\frac{C_{fs}^s \alpha_s \alpha_{fs}}{\alpha_{fs} - C_{fs}^s \alpha_s}(\mathbf{u}_s - \mathbf{u}_{fs})^2 \\
&+\nabla\cdot\left(\frac{(\alpha_f \mathbf{u}_f - (C_f^s - C_{fs}^s C_f^{fs})\alpha_s \mathbf{u}_s - C_f^{fs}\alpha_{fs}\mathbf{u}_{fs})^2}{\alpha_f - (C_f^s - C_{fs}^s C_f^{fs})\alpha_s - C_f^{fs}\alpha_{fs}}\right)\Bigg] \\
&-\frac{\alpha_f(\alpha_f - \rho_f P_3)}{2(\alpha_f P_1 - \alpha_{fs} P_3)}\nabla\cdot\frac{C_{fs}^s \alpha_s \alpha_{fs}}{\alpha_{fs} - C_{fs}^s \alpha_s}(\mathbf{u}_s - \mathbf{u}_{fs})^2,
\end{aligned}
\tag{59}
$$

where

$$
\begin{aligned}
I_1^8 &= \rho_f I_1^6 + \frac{(\alpha_f - \rho_f P_3)}{2} I_1^7, \\
I_2^8 &= \rho_f I_2^6 + \frac{(\alpha_f - \rho_f P_3)}{2} I_2^7, \\
I_3^8 &= \rho_f I_3^6 + \frac{(\alpha_f - \rho_f P_3)}{2} I_1^7, \\
\mathcal{V}_f &= \frac{(\alpha_f - \rho_f P_3)}{2} V_f^2 + \rho_f V_f^1.
\end{aligned}
$$

In (59), the inertial, pressure and gravity force terms take the usual structure. The change in fluid inertia due to its entrapment in solid and fine-solid is compensated by the two virtual mass force terms in the right hand side. However, if all the entrapments are ignored, the virtual mass forces also vanish and the momentum equation takes its original form.

3.2. Momentum equation for fine-solid

Adding (48) and (56), we get

$$
\begin{aligned}
0 = &-2\nabla p + \frac{\alpha_f \alpha_{fs}}{\alpha_f P_1 - \alpha_{fs} P_3}\left(\frac{d\mathbf{u}_f}{dt} - \frac{d\mathbf{u}_{fs}}{dt}\right) \\
&+\frac{\rho_s^e \alpha_s \alpha_{fs}}{\rho_s^e \alpha_s P_1 - \alpha_{fs}\alpha_s^e}\left(\frac{d\mathbf{u}_s}{dt} - \frac{d\mathbf{u}_{fs}}{dt}\right) \\
&+\left(\frac{\alpha_f I_1^1 - \alpha_{fs} I_1^6}{\alpha_f P_1 - \alpha_{fs} P_3} + \frac{\rho_s^e \alpha_s(\alpha_s I_1^1 - \alpha_{fs} I_1^2)}{\rho_s^e \alpha_s P_1 - \alpha_{fs}\alpha_s^e}\right)(\mathbf{u}_{fs} - \mathbf{u}_s) \\
&+\left(\frac{\alpha_f I_2^1 - \alpha_{fs} I_2^6}{\alpha_f P_1 - \alpha_{fs} P_3} + \frac{\rho_s^e \alpha_s(\alpha_s I_2^1 - \alpha_{fs} I_2^2)}{\rho_s^e \alpha_s P_1 - \alpha_{fs}\alpha_s^e}\right)(\mathbf{u}_f - \mathbf{u}_s) \\
&+\left(\frac{\alpha_f I_3^1 - \alpha_{fs} I_3^6}{\alpha_f P_1 - \alpha_{fs} P_3} + \frac{\rho_s^e \alpha_s I_3^1}{\rho_s^e \alpha_s P_1 - \alpha_{fs}\alpha_s^e}\right)(\mathbf{u}_f - \mathbf{u}_{fs}) \\
&+\frac{1}{\rho_s^e \alpha_s P_1 - \alpha_{fs}\alpha_s^e}\left(\rho_s^e \alpha_s V_{fs}^e + C_{fs}^s \alpha_s \rho_{fs}^e V_s^e - \rho_s^e \alpha_{fs} V_s^e\right) \\
&-\frac{1}{\alpha_f P_1 - \alpha_{fs} P_3}\left(\alpha_{fs} V_f^1 - \alpha_f\left(\frac{V_{fs}^e}{\rho_{fs}^e} + C_{fs}^s \frac{V_s^e}{\rho_s^e}\right)\right) \\
&+\frac{\alpha_{fs}}{\alpha_f P_1 - \alpha_{fs} P_3}\left[(C_f^s - C_{fs}^s C_f^{fs})\nabla\cdot(\alpha_s \mathbf{u}_s \mathbf{u}_s) + C_f^{fs}\nabla\cdot\alpha_{fs}\mathbf{u}_{fs}\mathbf{u}_{fs}\right.
\end{aligned}
$$

$$-\nabla\cdot(\alpha_f\mathbf{u}_f\mathbf{u}_f)+\nabla\cdot\left(\frac{(\alpha_f\mathbf{u}_f-(C_f^s-C_{fs}^sC_f^{fs})\alpha_s\mathbf{u}_s-C_f^{fs}\alpha_{fs}\mathbf{u}_{fs})^2}{\alpha_f-(C_f^s-C_{fs}^sC_f^{fs})\alpha_s-C_f^{fs}\alpha_{fs}}\right)$$
$$+\left(\frac{\rho_s^e\alpha_s}{\rho_s^e\alpha_sP_1-\alpha_{fs}\alpha_s^e}-\frac{\alpha_f-\alpha_{fs}}{\alpha_fP_1-\alpha_{fs}P_3}\right)\nabla\cdot\frac{C_{fs}^s\alpha_s\alpha_{fs}}{\alpha_{fs}-C_{fs}^s\alpha_s}(\mathbf{u}_s-\mathbf{u}_{fs})^2. \quad (60)$$

Multiplying (60) by $\left(\frac{\alpha_{fs}}{2\rho_{fs}}-\frac{P_1}{2}\right)$ and adding it with (43), we get the following **momentum equation for fine-solid with virtual mass forces.**

$$\rho_{fs}\left(\frac{\partial}{\partial t}(\alpha_{fs}\mathbf{u}_{fs})+\nabla\cdot\alpha_{fs}\mathbf{u}_{fs}\mathbf{u}_{fs}\right)=-\alpha_{fs}\nabla p+\rho_{fs}\alpha_{fs}\mathbf{g}$$
$$+\frac{\alpha_f\alpha_{fs}(\alpha_{fs}-\rho_{fs}P_1)}{2(\alpha_fP_1-\alpha_{fs}P_3)}\left(\frac{d\mathbf{u}_f}{dt}-\frac{d\mathbf{u}_{fs}}{dt}\right)$$
$$+\frac{\rho_s^e\alpha_s\alpha_{fs}(\alpha_{fs}-\rho_{fs}P_1)}{2(\alpha_{fs}\alpha_s^e-\rho_s^e\alpha_sP_1)}\left(\frac{d\mathbf{u}_{fs}}{dt}-\frac{d\mathbf{u}_s}{dt}\right)+I_1^9(\mathbf{u}_{fs}-\mathbf{u}_s)$$
$$+I_2^9(\mathbf{u}_f-\mathbf{u}_s)+I_3^9(\mathbf{u}_f-\mathbf{u}_{fs})+\mathcal{V}_{fs}$$
$$+\frac{\alpha_{fs}(\alpha_{fs}-\rho_{fs}P_1)}{2(\alpha_fP_1-\alpha_{fs}P_3)}\left[(C_f^s-C_{fs}^sC_f^{fs})\nabla\cdot(\alpha_s\mathbf{u}_s\mathbf{u}_s)+C_f^{fs}\nabla\cdot\alpha_{fs}\mathbf{u}_{fs}\mathbf{u}_{fs}\right.$$
$$\left.-\nabla\cdot(\alpha_f\mathbf{u}_f\mathbf{u}_f)+\nabla\cdot\left(\frac{(\alpha_f\mathbf{u}_f-(C_f^s-C_{fs}^sC_f^{fs})\alpha_s\mathbf{u}_s-C_f^{fs}\alpha_{fs}\mathbf{u}_{fs})^2}{\alpha_f-(C_f^s-C_{fs}^sC_f^{fs})\alpha_s-C_f^{fs}\alpha_{fs}}\right)\right]$$
$$+\left(\frac{\rho_s^e\alpha_{fs}(\alpha_{fs}-\rho_{fs}P_1)}{2(\rho_s^e\alpha_sP_1-\alpha_{fs}\alpha_s^e)}-\frac{(\alpha_f-\alpha_{fs})(\alpha_{fs}-\rho_{fs}P_1)}{2(\alpha_fP_1-\alpha_{fs}P_3)}+\rho_{fs}\right)$$
$$\times\nabla\cdot\frac{C_{fs}^s\alpha_s\alpha_{fs}}{\alpha_{fs}-C_{fs}^s\alpha_s}(\mathbf{u}_{fs}-\mathbf{u}_s)^2, \quad (61)$$

where

$$I_1^9=\frac{(\alpha_{fs}-\rho_{fs}P_1)}{2}\left(\frac{\alpha_fI_1^1-\alpha_{fs}I_1^6}{\alpha_fP_1-\alpha_{fs}P_3}+\frac{\rho_s^e\alpha_s(\alpha_sI_1^1-\alpha_{fs}I_1^2)}{\rho_s^e\alpha_sP_1-\alpha_{fs}\alpha_s^e}\right)+\rho_{fs}I_1^1,$$
$$I_2^9=\frac{(\alpha_{fs}-\rho_{fs}P_1)}{2}\left(\frac{\alpha_fI_2^1-\alpha_{fs}I_2^6}{\alpha_fP_1-\alpha_{fs}P_3}+\frac{\rho_s^e\alpha_s(\alpha_sI_2^1-\alpha_{fs}I_2^2)}{\rho_s^e\alpha_sP_1-\alpha_{fs}\alpha_s^e}\right)+\rho_{fs}I_2^1,$$
$$I_3^9=\frac{(\alpha_{fs}-\rho_{fs}P_1)}{2}\left(\frac{\alpha_fI_3^1-\alpha_{fs}I_3^6}{\alpha_fP_1-\alpha_{fs}P_3}+\frac{\rho_s^e\alpha_sI_3^1}{\rho_s^e\alpha_sP_1-\alpha_{fs}\alpha_s^e}\right)+\rho_{fs}I_3^1,$$
$$\mathcal{V}_{fs}=\frac{(\alpha_{fs}-\rho_{fs}P_1)}{2(\rho_s^e\alpha_sP_1-\alpha_{fs}\alpha_s^e)}\left(\rho_s^e\alpha_sV_{fs}^e+C_{fs}^s\alpha_s\rho_{fs}^eV_s^e-\rho_s^e\alpha_{fs}V_s^e\right)$$
$$-\frac{(\alpha_{fs}-\rho_{fs}P_1)}{2(\alpha_fP_1-\alpha_{fs}P_3)}\left(\alpha_{fs}V_f^1-\alpha_f\left(\frac{V_{fs}^e}{\rho_{fs}^e}+C_{fs}^s\frac{V_s^e}{\rho_s^e}\right)\right)$$
$$+V_{fs}^e\frac{\rho_{fs}}{\rho_{fs}^e}+C_{fs}^sV_s^e\frac{\rho_{fs}}{\rho_s^e}.$$

Also, in (61), the inertial, pressure and gravity force terms take their usual structure. The entrapments induced inertial changes are taken account by the two virtual mass force terms in the right hand side, which vanish if the entrapments are ignored.

3.3. Momentum equation for coarse-solid

Adding (48) and (57), we get

$$0=-2\nabla p+\frac{\alpha_s\alpha_f}{\alpha_f\alpha_s^e-\rho_s^e\alpha_sP_3}\left(\frac{d\mathbf{u}_f}{dt}-\frac{d\mathbf{u}_s}{dt}\right)$$
$$+\frac{\alpha_s\alpha_{fs}}{\rho_s^e\alpha_sP_1-\alpha_{fs}\alpha_s^e}\left(\frac{d\mathbf{u}_s}{dt}-\frac{d\mathbf{u}_{fs}}{dt}\right)$$
$$+\left(\frac{\rho_s^e(\alpha_fI_1^2-\alpha_sI_1^6)}{\alpha_f\alpha_s^e-\rho_s^e\alpha_sP_3}+\frac{\rho_s^e(\alpha_sI_1^1-\alpha_{fs}I_1^2)}{\rho_s^e\alpha_sP_1-\alpha_f\alpha_s^e}\right)(\mathbf{u}_{fs}-\mathbf{u}_s)$$
$$+\left(\frac{\rho_s^e(\alpha_fI_2^2-\alpha_sI_2^6)}{\alpha_f\alpha_s^e-\rho_s^e\alpha_sP_3}+\frac{\rho_s^e(\alpha_sI_2^1-\alpha_{fs}I_2^2)}{\rho_s^e\alpha_sP_1-\alpha_f\alpha_s^e}\right)(\mathbf{u}_f-\mathbf{u}_s)$$
$$+\left(\frac{\rho_s^e\alpha_sI_3^6}{\alpha_f\alpha_s^e-\rho_s^e\alpha_sP_3}+\frac{\rho_s^e\alpha_sI_3^1}{\rho_s^e\alpha_sP_1-\alpha_f\alpha_s^e}\right)(\mathbf{u}_f-\mathbf{u}_{fs})$$
$$+\frac{\rho_s^e\alpha_s}{\alpha_f\alpha_s^e-\rho_s^e\alpha_sP_3}\left[(C_f^s-C_{fs}^sC_f^{fs})\nabla\cdot(\alpha_s\mathbf{u}_s\mathbf{u}_s)+C_f^{fs}\nabla\cdot\alpha_{fs}\mathbf{u}_{fs}\mathbf{u}_{fs}\right.$$
$$\left.-\nabla\cdot(\alpha_f\mathbf{u}_f\mathbf{u}_f)+\nabla\cdot\left(\frac{(\alpha_f\mathbf{u}_f-(C_f^s-C_{fs}^sC_f^{fs})\alpha_s\mathbf{u}_s-C_f^{fs}\alpha_{fs}\mathbf{u}_{fs})^2}{\alpha_f-(C_f^s-C_{fs}^sC_f^{fs})\alpha_s-C_f^{fs}\alpha_{fs}}\right)\right]$$
$$+\left(\frac{\rho_s^e\alpha_s}{\rho_s^e\alpha_sP_1-\alpha_{fs}\alpha_s^e}-\frac{\rho_s^e\alpha_s}{\alpha_f\alpha_s^e-\rho_s^e\alpha_sP_3}\right)\nabla\cdot\frac{C_{fs}^s\alpha_s\alpha_{fs}}{\alpha_{fs}-C_{fs}^s\alpha_s}(\mathbf{u}_s-\mathbf{u}_{fs})^2$$
$$+\frac{1}{\rho_{fs}^e(\rho_s^e\alpha_sP_1-\alpha_{fs}\alpha_s^e)}\left(\rho_s^e\alpha_sV_{fs}^e+C_{fs}^s\alpha_s\rho_{fs}^eV_s^e-\rho_s^e\alpha_{fs}V_s^e\right)$$
$$-\frac{\rho_s^e}{\alpha_f\alpha_s^e-\rho_s^e\alpha_sP_3}\left(\alpha_sV_f^1-\alpha_f\frac{V_s^e}{\rho_s^e}\right)\cdot \quad (62)$$

Multiplying (62) by $\left(\frac{\alpha_s}{2\rho_s}-\frac{\alpha_s^e}{2\rho_s^e}\right)$ and adding it with (46), we get the following **momentum equation for (coarse-) solid with virtual mass forces**.

$$\rho_s\left(\frac{\partial}{\partial t}(\alpha_s\mathbf{u}_s)+\nabla\cdot(\alpha_s\mathbf{u}_s\mathbf{u}_s)\right)=-\alpha_s\nabla p+\rho_s\alpha_s\mathbf{g}$$
$$+\frac{\alpha_s\alpha_f(\alpha_s\rho_s^e-\alpha_s^e\rho_s)}{2(\alpha_f\alpha_s^e-\rho_s^e\alpha_sP_3)}\left(\frac{d\mathbf{u}_f}{dt}-\frac{d\mathbf{u}_s}{dt}\right)$$
$$+\frac{\alpha_s\alpha_{fs}(\alpha_s\rho_s^e-\alpha_s^e\rho_s)}{2(\alpha_{fs}\alpha_s^e-\rho_s^e\alpha_sP_1)}\left(\frac{d\mathbf{u}_{fs}}{dt}-\frac{d\mathbf{u}_s}{dt}\right)+I_1^{10}(\mathbf{u}_{fs}-\mathbf{u}_s)+I_2^{10}(\mathbf{u}_f-\mathbf{u}_s)$$
$$+I_3^{10}(\mathbf{u}_f-\mathbf{u}_{fs})+\mathcal{V}_s$$
$$+\frac{\alpha_s\rho_s^e-\alpha_s^e\rho_s}{2(\alpha_f\alpha_s^e-\rho_s^e\alpha_sP_3)}\left[(C_f^s-C_{fs}^sC_f^{fs})\nabla\cdot(\alpha_s\mathbf{u}_s\mathbf{u}_s)+C_f^{fs}\nabla\cdot\alpha_{fs}\mathbf{u}_{fs}\mathbf{u}_{fs}\right.$$
$$\left.-\nabla\cdot(\alpha_f\mathbf{u}_f\mathbf{u}_f)+\nabla\cdot\left(\frac{(\alpha_f\mathbf{u}_f-(C_f^s-C_{fs}^sC_f^{fs})\alpha_s\mathbf{u}_s-C_f^{fs}\alpha_{fs}\mathbf{u}_{fs})^2}{\alpha_f-(C_f^s-C_{fs}^sC_f^{fs})\alpha_s-C_f^{fs}\alpha_{fs}}\right)\right]$$
$$+\left(\frac{(\alpha_s\rho_s^e-\alpha_s^e\rho_s)\alpha_s}{2(\rho_s^e\alpha_sP_1-\alpha_{fs}\alpha_s^e)}-\frac{(\alpha_s\rho_s^e-\alpha_s^e\rho_s)\alpha_s}{2(\alpha_f\alpha_s^e-\rho_s^e\alpha_sP_3)}+\rho_s\right)$$
$$\times\nabla\cdot\frac{C_{fs}^s\alpha_s\alpha_{fs}}{\alpha_{fs}-C_{fs}^s\alpha_s}(\mathbf{u}_s-\mathbf{u}_{fs})^2, \quad (63)$$

where

$$I_1^{10}=\rho_sI_1^2+\frac{\rho_s^e(\alpha_s\rho_s^e-\alpha_s^e\rho_s)}{2}\left(\frac{\alpha_fI_1^2-\alpha_sI_1^6}{\alpha_f\alpha_s^e-\rho_s^e\alpha_sP_3}+\frac{\alpha_sI_1^1-\alpha_{fs}I_1^2}{\rho_s^e\alpha_sP_1-\alpha_f\alpha_s^e}\right),$$
$$I_2^{10}=\rho_sI_2^2+\frac{\rho_s^e(\alpha_s\rho_s^e-\alpha_s^e\rho_s)}{2}\left(\frac{\alpha_fI_2^2-\alpha_sI_2^6}{\alpha_f\alpha_s^e-\rho_s^e\alpha_sP_3}+\frac{\alpha_sI_2^1-\alpha_{fs}I_2^2}{\rho_s^e\alpha_sP_1-\alpha_f\alpha_s^e}\right),$$
$$I_3^{10}=\frac{\rho_s^e(\alpha_s\rho_s^e-\alpha_s^e\rho_s)}{2}\left(\frac{\alpha_sI_3^6}{\alpha_f\alpha_s^e-\rho_s^e\alpha_sP_3}+\frac{\alpha_sI_3^1}{\rho_s^e\alpha_sP_1-\alpha_f\alpha_s^e}\right),$$
$$\mathcal{V}_s=\frac{V_s^e\rho_s}{\rho_s^e}+\frac{(\alpha_s\rho_s^e-\alpha_s^e\rho_s)}{2\rho_{fs}^e(\rho_s^e\alpha_sP_1-\alpha_{fs}\alpha_s^e)}\left(\rho_s^e\alpha_sV_{fs}^e+C_{fs}^s\alpha_s\rho_{fs}^eV_s^e-\rho_s^e\alpha_{fs}V_s^e\right)$$
$$-\frac{(\alpha_s\rho_s^e-\alpha_s^e\rho_s)}{2(\alpha_f\alpha_s^e-\rho_s^e\alpha_sP_3)}\left(\rho_s^e\alpha_sV_f^1-\alpha_{fs}V_s^e\right). \quad (64)$$

Eq. (63) is analogous to (61) and (59) in structure. Although the expressions for drag coefficients and the viscous force are more complex in (64) than for fluid and fine-solid, they reduce to the usual structures if the entrapments are neglected. The momentum equations for fluid (59), fine-solid (61) and solid (63) ultimately take the form where the virtual mass force explicitly appear as the terms with the relative acceleration (difference of the Lagrangian temporal derivatives) between the two phases among the three. In the course of model development, there appeared complicated parameters depending on the linear and non-linear combinations of virtual mass coefficients. For the sake of simplicity, the non-linear combinations may be ignored. The advantage of this three-phase model development is that different rheologies can be used for the different phases in the viscous force terms.

4. Reduced virtual mass force coefficients

Another important feature of this model is that it can be reduced to pairwise two-phase mass flow model, including that analogous to

Pudasaini [9]. Instead of solid phase, if the gas bubbles are considered, the model reduces to that of Cook and Harlow [25]. Although the reduction of viscous and drag forces are also important aspects, here, we mainly focus on the reduction of virtual mass forces to two-phase. The possible reduction justifies that our model is more general than the existing two-phase models and also enables the comparison with them.

4.1. Virtual mass force coefficients with no fine-solid phase

Here, we ignore the fine-solid phase (i.e., $\alpha_{fs} = 0$) in the mixture so that all the C terms related to the fine-solid phase vanish. From the previous section, the reduced parameters are

$$P_1 = 0,$$
$$P_2 = \frac{1}{\rho_f}(\alpha_f - C_f^s\alpha_s),$$
$$P_3 = \frac{C_f^s(\alpha_s + C_f^s\alpha_s)}{\rho_s + C_f^s\rho_f} + \frac{\alpha_f - C_f^s\alpha_s}{\rho_f} = \frac{\rho_f C_f^s + \alpha_f\rho_s - C_f^s\alpha_s\rho_s}{\rho_f(\rho_s + C_f^s\rho_f)}.$$

Now, the coefficient of $\frac{d\mathbf{u}_f}{dt} - \frac{d\mathbf{u}_s}{dt}$ in (59) is reduced to

$$\begin{aligned}
&\frac{\rho_s^e\alpha_s\alpha_f(\alpha_f - \rho_f P_3)}{2(\alpha_f\alpha_s^e - \rho_s^e\alpha_s P_3)}\\
&= \frac{(\rho_s + C_f^s\rho_f)\alpha_s\alpha_f\left[\alpha_f - \dfrac{\rho_f C_f^s + \alpha_f\rho_s - C_f^s\alpha_s\rho_s}{\rho_s + C_f^s\rho_f}\right]}{2\left[\alpha_f(\alpha_s + C_f^s\alpha_s) - (\rho_s + C_f^s\rho_f)\alpha_s\dfrac{\rho_f C_f^s + \alpha_f\rho_s - C_f^s\alpha_s\rho_s}{\rho_f(\rho_s + C_f^s\rho_f)}\right]}\\
&= \frac{\rho_f\alpha_s\alpha_f(\rho_s\alpha_f + \rho_f C_f^s\alpha_f - \rho_f C_f^s - \rho_s\alpha_f + \rho_s C_f^s\alpha_s)}{2(\rho_f\alpha_f\alpha_s + \rho_f C_f^s\alpha_f\alpha_s - \rho_f C_f^s\alpha_s - \rho_s\alpha_s\alpha_f + \rho_s C_f^s\alpha_s\alpha_s)}\\
&= \frac{\rho_f\alpha_s\alpha_f(\rho_f C_f^s(\alpha_f - \alpha_s - \alpha_f) + \rho_s C_f^s\alpha_s)}{2(\rho_f\alpha_f\alpha_s + \rho_f C_f^s\alpha_s(\alpha_f - 1) - \rho_s\alpha_s\alpha_f + \rho_s C_f^s\alpha_s\alpha_s)}\\
&= \frac{\rho_f C_f^s\alpha_s\alpha_f\alpha_s(\rho_s - \rho_f)}{2(\rho_f\alpha_f\alpha_s - \rho_f C_f^s\alpha_s - \rho_s\alpha_s\alpha_f + \rho_s C_f^s\alpha_s\alpha_s)}\\
&= \frac{\rho_f C_f^s\alpha_s(\rho_s - \rho_f)\alpha_f\alpha_s}{2\alpha_s(\alpha_f(\rho_f - \rho_s) + C_f^s\alpha_s(\rho_s - \rho_f))}\\
&= -\frac{\rho_f C_f^s\alpha_f\alpha_s}{2(\alpha_f - C_f^s\alpha_s)}.
\end{aligned} \tag{65}$$

Similar reduction makes the coefficient of $\frac{d\mathbf{u}_f}{dt} - \frac{d\mathbf{u}_s}{dt}$ in (63):

$$\frac{\alpha_s\alpha_f(\alpha_s\rho_s^e - \alpha_s^e\rho_s)}{2(\alpha_f\alpha_s^e - \rho_s^e\alpha_s P_3)} = \frac{\rho_f C_f^s\alpha_f\alpha_s}{2(\alpha_f - C_f^s\alpha_s)}. \tag{66}$$

Eqs. (65) and (66) show that the sum of the virtual mass forces in the reduced two-phase flow is zero. On comparing with the coefficient of the relative acceleration of the virtual mass force term $\alpha_s\rho_f C$ in [9], the virtual mass coefficient in our model will take the form:

$$C = \frac{C_f^s\alpha_f}{2(\alpha_f - C_f^s\alpha_s).} \tag{67}$$

The structure of the model development in (66) says that the denominator must be sufficiently bounded away from zero. In fact, the fraction of entrapped fluid in solid must be substantially smaller than fluid fraction itself in the mixture. It is important to note that for dilute flow, α_s is (very) small, so is C_f^s. So, $\alpha_f \gg C_f^s\alpha_s$; and the coefficient in (66) $\approx \dfrac{C_f^s\rho_f\alpha_s\alpha_f}{2\alpha_f} = \dfrac{C_f^s\rho_f\alpha_s}{2} = \alpha_s\rho_f C$, where $C = \dfrac{1}{2}C_f^s$. This is the reduction to usual structure [9]. If $C_f^s = \dfrac{1 + 2\alpha_s}{2\alpha_f}$, this corresponds to the reduction to classical models. But, in our model, C_f^s can be chosen arbitrarily according to the material composition and flow situation.

4.2. Virtual mass force coefficients with no fluid phase

Next, we ignore the fluid phase (i.e., $\alpha_f = 0$) in the mixture so that all the C terms related to the fluid phase disappear. The flow is now akin to dry landslide. Here, we use the following reduced parameter.

$$P_1 = \frac{C_{fs}^s\alpha_s^e}{\rho_s^e} + \frac{\alpha_{fs} - C_{fs}^s\alpha_s}{\rho_{fs}^e} = \frac{\rho_{fs}C_{fs}^s + \alpha_{fs}\rho_s - C_{fs}^s\alpha_s\rho_s}{\rho_{fs}(\rho_s + C_{fs}^s\rho_{fs})}.$$

Now, the coefficient of $\frac{d\mathbf{u}_{fs}}{dt} - \frac{d\mathbf{u}_s}{dt}$ in (61) is reduced to

$$\frac{\rho_s^e\alpha_s\alpha_{fs}(\alpha_{fs} - \rho_{fs}P_1)}{2(\alpha_{fs}\alpha_s^e - \rho_s^e\alpha_s P_1)} = -\frac{\rho_{fs}C_{fs}^s\alpha_{fs}\alpha_s}{2(\alpha_{fs} - C_{fs}^s\alpha_s)}. \tag{68}$$

Similarly, the coefficient of $\frac{d\mathbf{u}_{fs}}{dt} - \frac{d\mathbf{u}_s}{dt}$ in (63) is reduced to

$$\frac{\alpha_s\alpha_{fs}(\alpha_s\rho_s^e - \alpha_s^e\rho_s)}{2(\alpha_{fs}\alpha_s^e - \rho_s^e\alpha_s P_1)} = \frac{\rho_{fs}C_{fs}^s\alpha_{fs}\alpha_s}{2(\alpha_{fs} - C_{fs}^s\alpha_s)}. \tag{69}$$

In this case also, due to the same coefficients with opposite sign, the sum of the virtual mass forces is zero. The coefficients are analogous to the previous reduction with no fine-solid phase.

4.3. Virtual mass force coefficients with no solid phase

Finally, we neglect the solid phase (i.e., $\alpha_s = 0$) in the mixture so that all the C terms related to the solid phase vanish. When the mixture contains only fluid and fine-sediments, the reduced parameters to be used will be:

$$P_1 = \frac{1}{\rho_{fs}^e}(1 + C_f^{fs})\alpha_{fs} = \frac{(1 + C_f^{fs})\alpha_{fs}}{\rho_{fs} + C_f^{fs}\rho_f},$$
$$P_2 = \frac{1}{\rho_f}(\alpha_f - C_f^{fs}\alpha_{fs}),$$
$$P_3 = \frac{C_f^{fs}(\alpha_{fs} + C_f^{fs}\alpha_{fs})}{\rho_{fs} + C_f^{fs}\rho_f} + \frac{\alpha_f - C_f^{fs}\alpha_{fs}}{\rho_f} = \frac{\rho_f C_f^{fs} + \alpha_f\rho_{fs} - C_f^{fs}\alpha_{fs}\rho_{fs}}{\rho_f(\rho_{fs} + C_f^{fs}\rho_f)}.$$

Then, the coefficient of $\frac{d\mathbf{u}_f}{dt} - \frac{d\mathbf{u}_{fs}}{dt}$ in (59) is reduced to

$$\frac{\alpha_f\alpha_{fs}(\alpha_f - \rho_f P_3)}{2(\alpha_f P_1 - \alpha_{fs}P_3)} = -\frac{\rho_f C_f^{fs}\alpha_f\alpha_{fs}}{2(\alpha_f - C_f^{fs}\alpha_{fs})}. \tag{70}$$

Similarly, the coefficient of $\frac{d\mathbf{u}_f}{dt} - \frac{d\mathbf{u}_{fs}}{dt}$ in (61) is reduced to

$$\frac{\alpha_f\alpha_{fs}(\alpha_{fs} - \rho_{fs}P_1)}{2(\alpha_f P_1 - \alpha_{fs}P_3)} = \frac{\rho_f C_f^{fs}\alpha_f\alpha_{fs}}{2(\alpha_f - C_f^{fs}\alpha_{fs})}. \tag{71}$$

Like in the previous two reductions, here also the analogous virtual mass coefficients show that the virtual mass forces balance each other.

Thus, we proved that at least in the reduced situations of two-phases (solid and fluid; solid and fine-solid; fine-solid and fluid), the pairwise sums of virtual mass forces become zero. Moreover, the reduced virtual mass coefficients in all the three cases are symmetrical. When one is known, others can be obtained. This formally proves the consistency of our derivations, although it was rather complex.

5. Simulation of two-phase debris flow using new virtual mass coefficient

Here we employ the new reduced virtual mass coefficient obtained in (66) to simulate the two-phase debris flow as a mixture of solid particles and viscous fluid (s, fs) that moves down an inclined plane followed by a horizontal run out. Moreover, to reveal the effect of new virtual mass coefficients on flow-obstacle-interaction, an integrated obstacle system that consists of a forward-facing tetrahedron followed by two other tetrahedra is installed in the flow lines. All the initial and boundary conditions, the numerical integration techniques, the

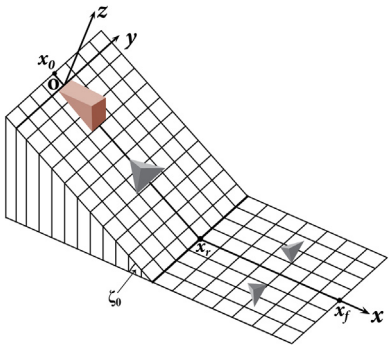

Fig. 2. Initial set up showing the flow domain, that starts with a slope from $x_0 = -25$ to $x_r = 160$ m inclined at an angle of $\zeta_0 = 45°$ with the horizontal, followed by a horizontal run out from $x_r = 160$ to $x_f = 450$ m; $-200 \le y \le 200$ m; O is the origin. The initial debris (75% solid and 25% fluid) in brown encounters a tetrahedral obstacle in gray when it is triggered and flows downstream to interact with two more tetrahedra downstream [11].

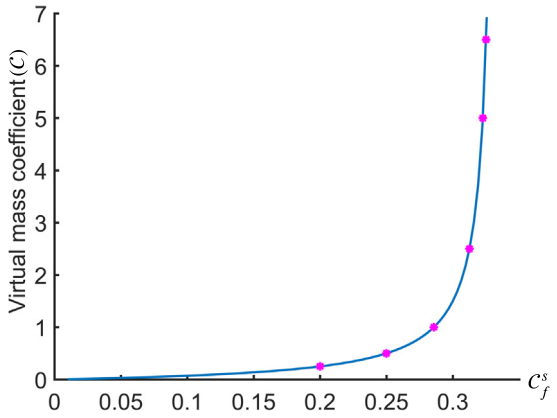

Fig. 3. For $\alpha_s = 0.75$, the reduced virtual mass coefficient C for solid and fluid as given by (67) increases along with the entrapment coefficient C_f^s.

employed model [9], and the chosen parameters are same as those used in [11], except that the virtual mass coefficient was a constant value of $C = 0.4$ in [11]. As in [9], Mohr–Coulomb plasticity is employed to address the solid-phase deformation, whereas there are both Newtonian and solid volume fraction gradient enhanced non-Newtonian contributions to the fluid phase rheology. The details of the employed general two-phase mass flow model and the Total Variation Diminishing (TVD) Non-Oscillatory Central (NOC) schemes can be respectively found in [9] and [19], which we do not explain here. However, here, we briefly describe the initial set-up (Fig. 2).

The spatial domain for simulation is $[-25, 450] \times [-200, 200]$ m. The debris mass is kept in the form of a triangular wedge with base at $[0, 50] \times [-15, 15]$ m that contains a homogeneous mixture of solid (75%) and fluid (25%). When the debris mass is released, it slides down the plane inclined at an angle of $\zeta_0 = 45°$ to $x_r = 160$ m, that follows a horizontal run out zone to $x_f = 450$ m. A stationary obstacle is in the form of a forward-facing triangular pyramid (tetrahedron) having a triangular base with $(70, 0, 0)$ m as the foremost point and the remaining two vertices at $(110, -24, 0)$ m and $(110, 24, 0)$ m. The apex of the tetrahedron is at $(90, 0, 30)$ m. The other two downstream pyramids are smaller in size and are oriented at $\pm 8.13°$ from the x-axis so as to keep them almost in the flow lines. These two pyramids have the vertices of the triangular bases at $(178, \pm 70, 0)$ m, $(212, \pm 54, 0)$ m and $(204, \pm 98, 0)$ m, and their apices are at $(192, \pm 72, 15)$ m (Fig. 2). The base and the height of these two pyramids are halved since they are to interact the debris lobes with reduced mass divided into two halves due to the first tetrahedron.

In natural debris flows and other mass flows, the solid and fluid constituents may occupy different volume fractions in the different parts of the flowing body. As simulated here and in [11], solid and fluid respond differently with obstacles; more solid is held momentarily than fluid by obstacles. This is also observed in real field scenario. To highlight the effect of newly developed virtual mas coefficient through numerical experiments, we have chosen relatively more complicated set up that contains an inclined surface followed by a horizontal run out with three obstacles mounted in the flow path. Since the expression for the virtual mass coefficient as given by (66) clearly depends upon the solid (also fluid) volume fraction (α_s) and the fraction of fluid entrapped in solid (C_f^s), the virtual mass coefficient is a dynamical variable that evolves differently in different parts of the flowing body. Even the classical virtual mass coefficient, $C = \dfrac{1 + 2\alpha_s}{2(1 - \alpha_s)}$ depends on α_s [9,16,17,26]. However, to estimate the appropriate value of C_f^s, we take the help of the initial material constituents. For given $\alpha_s = 0.75\,(\alpha_f = 0.25)$, (67) shows that C_f^s must be less than 0.33 for a bounded value of C.

Fig. 3 shows the change in virtual mass force coefficient C as a function of the entrapment coefficient C_f^s. Some typical values of $C_f^s = [0.325, 0.322, 0.3125, 0.2857, 0.25, 0.2]$ correspond to $C = [6.5, 5, 2.5, 1, 0.5, 0.25]$, which are marked in Fig. 3. Fig. 4 presents the simulation result for the debris flow-obstacle-interaction with the same set-up as described in the previous paragraph but with the mew virtual mass coefficient given by (66) with the portion of fluid entrapped in solid having value 0.325 (i.e., $C_f^s = 0.325$). This gives the virtual mass coefficient $C = 6.5$. When the initial debris mass collapses, it advects downslope and spreads across due to gravity and pressure. Although the flow dynamics and obstacle-interactions for solid (Left panels, A), fluid (Middle panels, B) and total debris bulk (Right panels, C) are qualitatively similar to those presented in [11], there are some quantitative differences between the amount of fluid deflected by the obstacle. We briefly describe the main observations. The debris flow already begins to interact with the first obstacle at $t = 2$ s. The frontal nose of the first tetrahedron begins to deflect the flow and the deflection continues as time progresses. Debris vacuum is created behind the obstacle. The two deflected debris lobes begin to interact with the two downstream pyramids at $t = 6$ s. The obstacles obstruct more solid than fluid and more solid is momentarily held by the obstacles than fluid. As solid and fluid have different mechanics and rheology, they possess different dynamical interactions with obstacles. As the solid phase is denser than fluid and due to its frictional nature, more solid begins to deposit around the front nose of the obstacles than fluid. More solid is deflected towards the outer flanks of the downstream pyramids whereas more fluid is deflected inward, resulting in significant phase-separation. A close scrutiny shows that the phase-separation begins at $t = 6$ s and is more intensified as time progresses. At $t = 13$ s, major portion of the solid is deflected outwards and only a minor portion is deflected inward. On contrary, major portion of fluid is deflected inward and a minor portion is deflected outward. Fluid moves more downslope than solid. Moreover, for fluid, the inward deflected lobes travel more downslope than the outward deflected lobes. Due to the increased virtual mass coefficient, more fluid has been deflected outward along with the solid than in [11]. Here, we only presented some qualitative description of the flow-obstacle-interaction. The detailed qualitative and quantitative descriptions of the flow-obstacle interactions, the reasons for the phase-separation, and advantages of such obstacle arrangements have been explained in [11].

In the next simulation (Fig. 5), we choose relatively lower value $C_f^s = 0.2$ meaning that less fraction of fluid is entrapped in solid in comparison to the previous simulation (Fig. 4). This gives the decreased virtual mass coefficient $C = 0.25$. The obstacle-interaction is different in these two simulations and the difference is more pronounced for $t > 10$ s. Solid is completely deflected outward, whereas entire fluid is

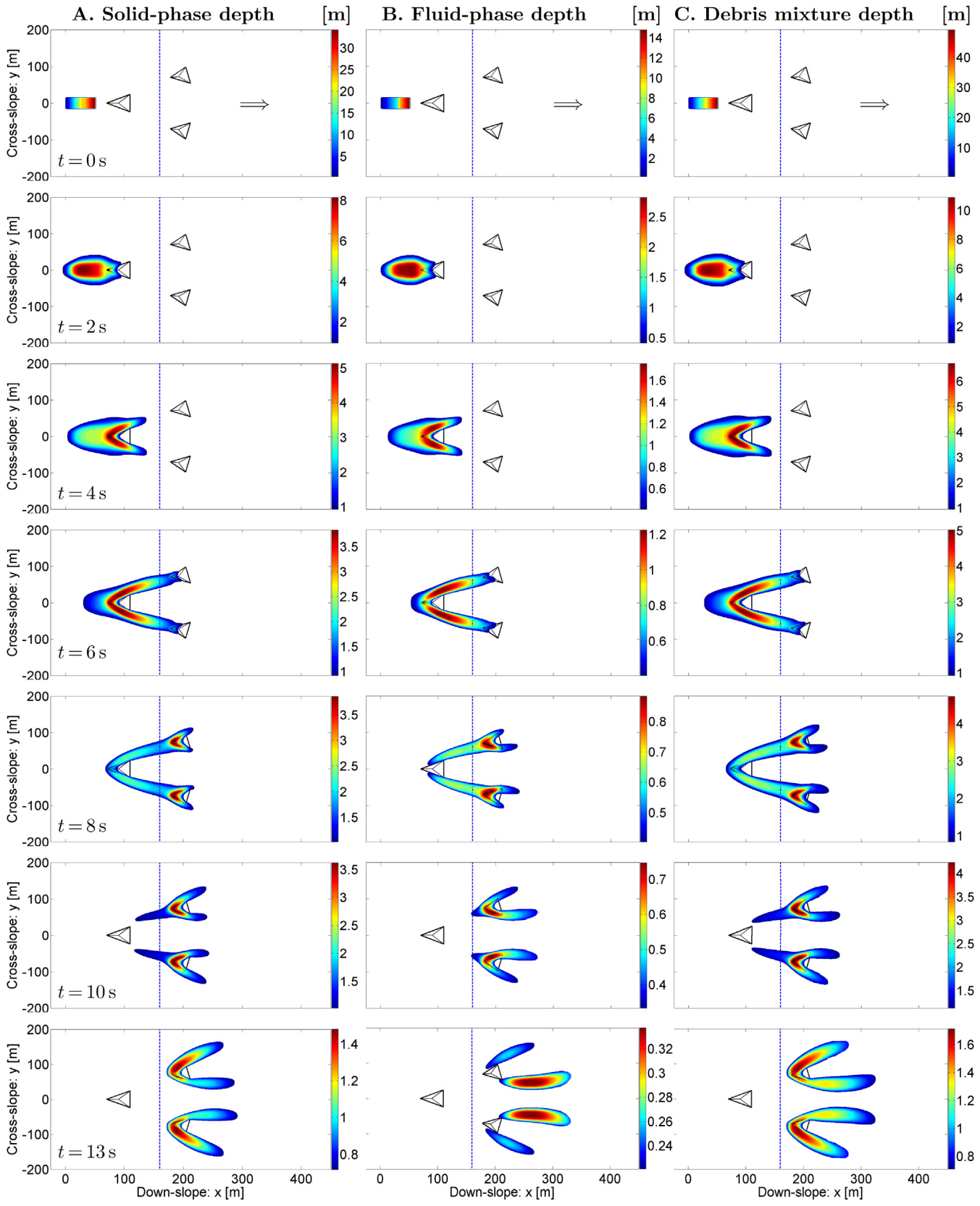

Fig. 4. Time evolution and flow-obstacle-interaction of **A.** Solid phase, **B.** Fluid phase, **C.** Total debris mixture with new virtual mass coefficient $C = \dfrac{C_f^s \alpha_f}{2(\alpha_f - C_f^s \alpha_s)} = 6.5$, where $C_f^s = 0.325$. When the debris flow is triggered, it hits a forward facing tetrahedral obstacle followed by two more smaller tetrahedra in the flow lines. Major portion of solid is directed outwards whereas major portion of fluid is directed inwards.

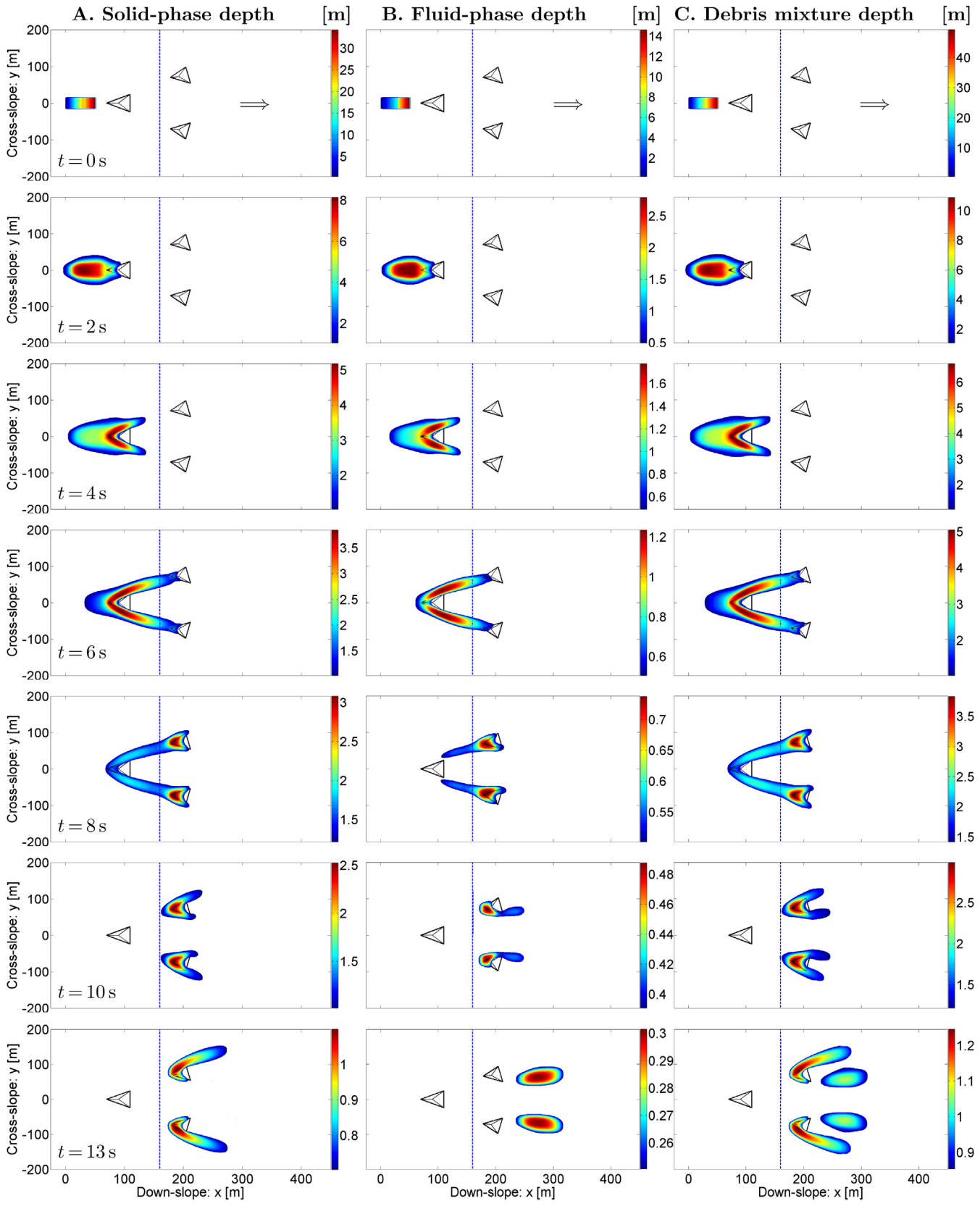

Fig. 5. Time evolution and flow-obstacle-interaction of **A.** Solid phase, **B.** Fluid phase, **C.** Total debris mixture with new virtual mass coefficient $C = \frac{C_f^s \alpha_f}{2(\alpha_f - C_f^s \alpha_s)} = 0.25$, where $C_f^s = 0.2$. When the debris flow is triggered, it hits a forward facing tetrahedral obstacle followed by two more smaller tetrahedra in the flow lines. The flow-obstacle-interactions are different from Fig. 4. Due to less coupling, solid and fluid move more independently.

deflected inward in Fig. 5 ($t = 13$ s). Also in this case, we observe that inward fluid lobes travel more downslope than the outward solid lobes. The phase-separation is more pronounced in Fig. 5 than in Fig. 4. Since less fraction of fluid is entrapped in solid, it provides less hindrance to solid, so solid and fluid can flow more independently due to less coupling.

From these two simulation results, we observe that the new reduced virtual mass coefficients can capture the dynamics and flow-obstacle-interactions of two-phase mass flow. Any empirical value of the virtual mass coefficient or the corresponding value given by the classical expression can be made equivalent to some appropriate choice of C_f^s in the newly developed virtual mass coefficient. This also validates the new model. As arbitrary value can be assigned to our C_f^s, even the newly developed reduced virtual mass coefficients are more general to those in the existing two-phase mass flow model [9].

Although there are some internal factors like flow density, nature of the dispersed particles, and the particle size distribution to influence the phase-separation, the phase-separation as simulated here is due to the external factors, especially the boundary conditions–obstacle induced change in topographic slope to especially affect the velocity profile. The energy dissipating defense structures not only reduce and redirect the debris flow velocity, but also initiate phase-separation [9,11,13,15]. The simulation results presented here show that different virtual mass coefficients can bring different degree and pattern of phase-separation. Wang et al. [13] experimentally showed that the values of debris flow density have significant influence on phase-separation in debris flows. The changing effective density in our multiphase model formulation is associated with the entrapment coefficients and the constituent fractions. This plays important role in phase-separation.

6. Discussion and summary

Here, we modeled a debris flow as a multiphase mass flow with three distinct phases, namely coarse-solid, fine-solid and viscous fluid. We also considered the fraction of fluid entrapped in solid and fine-solid along with fraction of fine-solid entrapped in solid. This resulted in a total of six fields in the model development. Analogous to virtual mass coefficients, we introduced three linear functions to relate the portion and velocities of the entrapped fields in the host fields. By these coefficients, we also related bulk fluid and bulk fine-solid momenta with the solid, total fine-solid and total fluid momenta. From the separate mass and momentum balances of the three bulk phases (coarse-solid, fine-solid and fluid) and three entrapped fields (fine-solid entrapped in coarse-solid, fluid entrapped in coarse-solid, and fluid entrapped in fine-solid), we could construct the mass and momentum balances for the three phases. In fact, mass balance equations of each bulk phase and the fields entrapped on it are combined to give three mass balance equations for the three phases. Source terms of each momentum equation of the three phases and the three entrapped fields include pressure, gravity, drag and viscous forces. Solid momentum equation and the other two momentum equations of the fluid-type material entrapped on it are combined to form an intermediate momentum equation for the solid phase, where the enhanced density of solid appears in the inertial and gravity terms, and enhanced or effective solid volume fraction in the pressure term. Viscous force has also been enhanced, which we called it as the effective viscous force for solid. All the effective force terms would reduce to the usual force terms in case if the entrapments are ignored. Similar process has been adopted for the fine-solid momentum equation. In the intermediate momentum equation of each phase, there appeared the flux terms of other phases, which were later removed. The momentum equations with enhanced densities are further processed to obtain those with usual phase densities. Initially, the momentum balance equations did not contain the virtual mass force terms explicitly. Later, in due course of model formulation, three different virtual mass forces evolved in the momentum equations. Since three phases are involved and there are three different entrapments, the process of deriving the momentum balance equations with virtual mass forces demanded longer procedure with more complicated parameters than the existing two-phase models. Virtual mass force coefficients induced enhanced viscosities, phase fractions, drags, viscous stresses and gravity forces of the coarse-solid and fine-solid are the novel aspects of the model. The newly constructed model, and especially the virtual mass forces reduce to the existing two-phase models [9,25]. An important and interesting observation is that the new virtual mass coefficients sum to zero. Another advantage of the model is that the viscous and drag terms are generic and one can use the suitable rheology for the materials involved, and the drag formulations in the multiphase flow.

To reveal the importance and effectiveness of the newly developed virtual mass coefficients, we employed the reduced virtual mass coefficient for solid and fluid to numerically integrate the general two-phase mass flow model [9] with the initial set-ups and other parameter selection as in [11]. With appropriately chosen two different values of the portion of fluid entrapped in solid, simulations produced different flow-obstacle-interactions and dynamically different phase-separation. Simulations also revealed that any empirical value or the expression for the virtual mass coefficient in two-phase mass flow model [9] can be recovered by the appropriate choice of the portion of fluid entrapped in solid. Thus, such entrapment coefficient makes our virtual mass forces, even in reduced form, more general than those found in existing literatures.

List of symbols

C_f^s	Fraction of fluid entrapped in solid
C_f^{fs}	Fraction of fluid entrapped in fine-solid
C_{fs}^s	Fraction of fine-solid entrapped in solid
f	Fluid phase
fs	Fine-solid phase
g	Magnitude of acceleration due to gravity
$\mathbf{g}$	Acceleration due to gravity
I_i^j	$i = 1, 2, 3; j = 1, 2, \ldots, 10$ binary drag coefficients
K	General interfacial momentum transfer, drag
K_1^{j}	Drag between field i and field j; the fields are fluid (f), fine-solid (fs), solid (s), fluid entrapped in solid (f-es), fluid entrapped in fine-solid (f-efs), fine-solid entrapped in solid (fs-es)
p	Pressure
P_1, P_2, P_3	Coefficients of pressure gradient in (43), (53), (55)
s	Solid phase
$\bar{\mathbf{u}}_f$, $\bar{\mathbf{u}}_{fs}$, $\bar{\mathbf{u}}_s$	Velocity of bulk fluid, fine-solid, solid
$\mathbf{u}_{fs}^{e_s}$	Velocity of fine-solid entrapped in solid
$\mathbf{u}_f^{e_s}$	Velocity of fluid entrapped in solid
$\mathbf{u}_f^{e_{fs}}$	Velocity of fluid entrapped in fine-solid
$\mathbf{u}_f$	Velocity of fluid phase
$\mathbf{u}_{fs}$	Velocity of fine-solid phase
$\mathbf{u}_s$	Velocity of solid phase
V_f, V_{fs}, V_s	Viscous forces for solid, fine-solid and fluid
$\mathcal{V}_f$, $\mathcal{V}_{fs}$, $\mathcal{V}_s$	Viscous forces for fluid, fine-solid and solid in (59), (61) and (63)
V_f^1, V_f^2	Viscous forces in the intermediate Eqs. (55) and (58)

$V_f^{e_s}$, $V_{fs}^{e_s}$	Momentum transport due to viscosity of fluid and fine-solid entrapped in solid
$V_f^{e_{fs}}$	Momentum transport due to the viscosity of fluid entrapped in fine-solid
V_{fs}^{e}, V_s^{e}	Effective viscous forces for fine-solid and solid
α_f, α_{fs}, α_s	Fluid, fine-solid and solid volume fractions in the mixture
$\bar{\alpha}_f$, $\bar{\alpha}_{fs}$, $\bar{\alpha}_s$	Portion of fluid, fine-solid and solid in their own bulks
$\alpha_f^{e_s}$, $\alpha_{fs}^{e_s}$	Portion of the fluid and fine-solid entrapped in solid
$\alpha_f^{e_{fs}}$	Portion of the fluid entrapped in fine-solid
α_{fs}^{e}, α_s^{e}	Effective fine-solid and solid volume fraction in the mixture
α_i	Total volume fraction of the phases i ($i = s$, fs or f)
ρ_f, ρ_{fs}, ρ_s	Densities for fluid, fine-solid and solid phases
ρ_{fs}^{e}, ρ_s^{e}	Effective fine-solid and solid densities
∇	Gradient operator
$\frac{d}{dt}$	Material time derivative

CRediT authorship contribution statement

Parameshwari Kattel: Model expansion, Simulation, Explanations, Completion of the paper writing. **Khim B. Khattri:** Model expansion, Explanations, improvements of the paper. **Shiva P. Pudasaini:** Generated the model concept, Derived the basic model, Made the basic draft, Did internal revision, Supervision.

Declaration of competing interest

The authors declare that they have no known competing financial interests or personal relationships that could have appeared to influence the work reported in this paper.

Acknowledgments

The authors are grateful to the reviewers and the Editor, Professor Giuseppe Saccomandi for their constructive comments for the substantial improvement of the paper. Shiva P. Pudasaini gratefully acknowledges the financial support provided by the German Research Foundation (DFG) through the research project, PU 386/5-1: "A novel and unified solution to multi-phase mass flows": U_MultiSol.

Appendix A. Supplementary materials

Supplementary material related to this article can be found online at https://doi.org/10.1016/j.ijnonlinmec.2020.103638.

References

[1] R.M. Iverson, The physics of debris flows, Rev. Geo-Phys. 35 (3) (1997) 245–296.
[2] T. de Haas, L. Braat, J.R.F.W. Leuven, I.R. Lokhorst, M.G. Kleinhans, Effects of debris flow composition on runout, depositional mechanisms, and deposit morphology in laboratory experiments, J. Geophys. Res. Earth Surf. 120 (2015) 1949–1972.
[3] T. de Haas, T. van Woerkom, Bed scour by debris flows: Experimental investigation of effects of debris-flow composition, Earth Surf. Process. Landf. 41 (13) (2016) 1951–1966.
[4] S.P. Pudasaini, M. Mergili, A multi-phase mass flow model, J. Geophys. Res.: Earth Surf. 124 (2019) 2920–2942, http://dx.doi.org/10.1029/2019JF005204.
[5] S.P. Pudasaini, M. Krautblatter, A two-phase mechanical model for rock-ice avalanches, J. Geophys. Res. Earth Surf. 119 (2014) http://dx.doi.org/10.1002/2014JF003183.
[6] M. Mergili, M. Jaboyedoff, J. Pullarello, S.P. Pudasaini, Back calculation of the 2017 Piz Cengalo-Bondo landslide cascade with r.avaflow: what we can do and what we can learn, Nat. Hazards Earth Syst. Sci. 20 (2020) 505–520, http://dx.doi.org/10.5194/nhess-20-505-2020.
[7] T. Takahashi, Debris Flow, in: IAHR-AIRH Monograph Series A. Balkema, Rotterdam, Netherlands, 1991.
[8] E.B. Pitman, L. Le, A two fluid model for avalanche and debris flows, Phil. Trans. R. Soc. A 363 (3) (2005) 1573–1601.
[9] S.P. Pudasaini, A general two-phase debris flow model, J. Geophys. Res. 117 (2012) F03010, http://dx.doi.org/10.1029/2011JF002186.
[10] S.P. Pudasaini, A full description of generalized drag in mixture mass flows, Eng. Geol. 265 (2020) http://dx.doi.org/10.1016/j.enggeo.2019.105429.
[11] P. Kattel, J. Kafle, J.-T. Fischer, M. Mergili, B.M. Tuladhar, S.P. Pudasaini, Interaction of two-phase debris flow with obstacles, Eng. Geol. 242 (2018) 197–217.
[12] P. Kattel, B.M. Tuladhar, Interaction of two-phase debris flow with lateral converging shear walls, J. Nepal Math. Soc. 1 (2) (2018) 40–52.
[13] F. Wang, J. Wang, X. Chen, J. Chen, The influence of temporal and spatial variations on phase separation in debris flow deposition, Landslide 16 (2019) 497–514, http://dx.doi.org/10.1007/s10346-018-1119-5.
[14] S.P. Pudasaini, J.-T. Fischer, A mechanical erosion model for two-phase mass flows, Int. J. Multiph. Flow. (2020) http://dx.doi.org/10.1016/j.ijmultiphaseflow.2020.103416.
[15] S.P. Pudasaini, J.-T. Fischer, A mechanical model for phase-separation in debris flow, Int. J. Multiph. Flow. (2020) http://dx.doi.org/10.1016/j.ijmultiphaseflow.2020.103292.
[16] M. Ishii, N. Zuber, Drag coefficient and relative velocity in bubbly, droplet or particulate flows, Amer. Inst. Chem. Eng. J. 25 (5) (1979) 843–855.
[17] D. Drew, Mathematical modelling of two-phase flows, Annu. Rev. Fluid Mech. 15 (1983) 261–291.
[18] T. Zwinger, A. Kluwick, P. Sampl, Numerical simulation of dry-snow avalanche flow over natural terrain, in: K. Hutter, N. Kirchner (Eds.), Dynamic Response of Granular and Porous Materials under Large and Catastrophic Deformations, in: Lecture Notes in Appl. and Comput. Mech., vol. 11, Springer, Berlin, 2003, pp. 161–194.
[19] S.P. Pudasaini, K. Hutter, Avalanche Dynamics: Dynamics of Rapid Flows of Dense Granular Avalanches, Springer, New York, 2007, p. 602.
[20] P. Kattel, K.B. Khattri, P.R. Pokhrel, J. Kafle, B.M. Tuladhar, S.P. Pudasaini, Simulating glacial lake outburst floods with a two-phase mass flow model, Ann. Glaciol. 57 (71) (2016) 349–358.
[21] M. Mergili, J.T. Fischer, J. Krenn, S.P. Pudasaini, R.avaflow v1, an advanced open source computational framework for the propagation and interaction of two-phase mass flows, Geosci. Model Dev. 10 (2017) 553–569, http://dx.doi.org/10.5194/gmd-10-553-2017.
[22] M. Pailha, O. Pouliquen, A two-phase flow description of the initiation of underwater granular avalanches, J. Fluid Mech. 633 (2009) 115–135.
[23] S.P. Pudasaini, A fully analytical model for virtual mass force in mixture flows, Int. J. Multiph. Flow. 113 (2019) 142–152.
[24] D. Drew, L. Cheng, R.T. Lahey Jr., The analysis of virtual mass effects in two-phase flow, Int. J. Multiph. Flow. 3 (1979) 233–242.
[25] T.L. Cook, F.H. Harlow, Virtual mass in multiphase flow, Int. J. Multiph. Flow. 10 (1984) 691–696.
[26] D.A. Drew, R.T. Lahey Jr., The virtual mass and lift force on a sphere in rotating and straining inviscid flow, Int. J. Multiph. Flow. 13 (1) (1987) 113–121.
[27] T. Watanabe, Y. Kukita, The effect of the virtual mass term on the stability of the two-fluid model against perturbations, Nucl. Eng. Des. 135 (1992) 327–340.
[28] C.I. Kleinstreuer, Two-Phase Flow: Theory and Applications, CRC Press, 2003, p. 512.
[29] C.R. Maliska, E.E. Paladino, The role of virtual mass, lift and wall lubrication forces in accelerated bubbly flows, in: Energy: Production, Distribution and Conservation-Milan 2006, 2006, pp. 953–962.
[30] M. Ishii, Two-fluid model for two-phase flow, Multiph. Sci. Technol. 5 (1990) 1–65.
[31] L. Cheng, R.T. Lahey Jr., D.A. Drew, The effect of virtual mass on the prediction of critical flow, in: Proc. 3rd CSNI Specialist Meeting, Transient Two-Phase Flow, Hemisphere, Washington, 1983, pp. 323–340.
[32] R.T. Lahey Jr., L.Y. Cheng, D.A. Drew, J.E. Flaherty, The effect of virtual mass on the numerical stability of accelerating two-phase flows, in: Annual Meeting of American Institute of Chemical Engineers Paper No. 56b, Florida, 12-16 November, 1978.
[33] H.C. No, M.S. Kazimi, Effect of virtual mass on the mathematical characteristics and numerical stability of the two-fluid model, Nucl. Sci. Eng. 89 (1985) 197–206.
[34] H. Lamb, Hydrodynamics, Cambridge University Press, Cambridge, 1952, pp. 160–201.
[35] L. Prandtl, Essentials of Fluid Dynamics, Blackie & Son, Glasgow, 1952.
[36] N.H. Thomas, T.R. Auton, K. Sene, J.C.R. Hunt, Entrapment and transport of bubbles by transient large eddies in multiphase turbulent shear flows, in: International Conference on the Physical Modelling of Multi-Phase Flow, Coventry, England, 19-21 April, 1983.
[37] A. Biesheuvel, S. Spoelstra, The added mass coefficient of a dispersion of spherical gas bubbles in liquid, Int. J. Multiph. Flow. 15 (6) (1989) 911–924.
[38] K. Sankaranarayanan, X. Shan, I.G. Kevrekidis, S. Sundaresan, Analysis of drag and virtual mass forces in bubbly suspensions using an implicit formulation of the lattice Boltzmann method, J. Fluid Mech. 452 (2002) 61–96.

[39] M. Simcik, M.C. Ruzicka, J. Drahoš, Computing the added mass of dispersed particles, Chem. Eng. Sci. 63 (2008) 4580–4595.
[40] L.M. Milne-Thomson, Theoretical Hydrodynamics, MacMillan, London, 1968, pp. 488–491.
[41] R.G. Dong, Effective Mass and Damping of Submerged Structures, Lawrence Livermore Laboratory, University of California Livermore, 1978, California 94550, UCRL-52342.
[42] D. Zhang, N.G. Deen, J.A.M. Kuipers, Numerical simulation of the dynamic flow behavior in a bubble column: A study of closures for turbulence and interface forces, Chem. Eng. Sci. 61 (2006) 7593–7608.
[43] B. Domnik, S.P. Pudasaini, R. Katzenbach, S.A. Miller, Coupling of full two-dimensional and depth-averaged models for granular flows, J. Non-Newton. Fluid Mech. 201 (2013) 56–68.
[44] A. von Boetticher, J.M. Turowski, B.W. McArdell, D. Rickenmann, J.W. Kirchner, DebrisInterMixing-2.3: A finite volume solver for three-dimensional debris-flow simulations with two calibration parameters-Part 1: Model description, Geosci. Model Dev. 9 (2016) 2909–2923, http://dx.doi.org/10.5194/gmd-9-2909-2016, www.geosci-model-dev.net/9/2909/2016/.
[45] J.E. Warren, P.J. Root, The behaviour of naturally fractured reservoirs, Soc. Pet. Eng. J. 3 (1963) 245–255.
[46] T. Arbogast, J. Douglas Jr., U. Hornung, Derivation of the double porosity model of single phase via homogenization theory, SIAM J. Math. Anal. 21 (4) (1990) 823–836.
[47] A. Bourget, S. Luckhaus, A. Mikelić, Convergence of the homogenization process for a double porosity model of immiscible two-phase flow, SIAM J. Math. Anal. 27 (6) (1996) 1520–1543.
[48] G.R. Jerauld, S.J. Salter, The effect of pore-structure on hysteresis in relative permeability and capillary pressure: Pore-level modeling, Transp. Porous Media 5 (1990) 103–151.
[49] P. Kordulová, M. Beneš, Solutions to the seepage face model for dual porosity flows with hysteresis, Nonlinear Anal. 75 (2012) 6473–6484.
[50] B. Domnik, S.P. Pudasaini, Full two-dimensional rapid chute flows of simple viscoplastic granular materials with a pressure-dependent dynamic slip-velocity and their numerical simulations, J. Non-Newton. Fluid Mech. 173–174 (2012) 72–86.
[51] P.R. Pokhrel, K.B. Khattri, B.M. Tuladhar, S.P. Pudasaini, A generalized quasi two-phase bulk mixture model for mass flow, Int. J. Non-Linear Mech. 199 (2018) 229–239.
[52] K.B. Khattri, S.P. Pudasaini, An extended quasi two-phase mass flow model, Int. J. Non-Linear Mech. 106 (2018) 205–222.